the 16c sites, with a B_{iso} factor arbitrarily fixed at 1.0 $Å^2$. The isotropic temperature factors of the vanadium and the oxide ions were refined, as were the anion position coordinates.

In the following cycle, the lithium ions were allowed to occupy both the tetrahedral 8a and the octahedral 16c sites, whereas the vanadium cations were distributed over the octahedral 16c and 16d sites. The total contents of lithium and vanadium ions were both fixed to 2.0, in accordance with the formula $Li_2V_2O_4$.

In the refined structure, which gave a reliability factor of 6.5%, 1.9(3) lithium ions are situated in the octahedral 16c sites, and 0.1(3) in the tetrahedral 8a sites. Although most of the vanadium ions, viz. 1.93(4), occupy the 16d sites, as in the spinel $Li[V_2]O_4$, a small fraction (0.07(4)) is found in the 16c sites. These values are in good agreement with the vanadium distribution obtained for $Li_{1.5}V_2O_4$, and confirm lithium-deficiency in the starting material, with a structure of the type $(Li_{0.93}V_{0.07})8a[V_{1.93}\square_{0.07}]O_4$. The full structural parameters of $Li_2V_2O_4$ are listed in Table 6.7a, the observed and calculated intensities in Table 6.7b.

This model indicates that, within experimental error, for the composition $Li_2V_2O_4$, all the lithium cations are situated in the octahedral 16c sites. The structure of $Li_2V_2O_4$ is thus a partially ordered rocksalt phase, where all the lithium cations are situated in the 16c sites (vacant in spinels) and the vanadium cations reside in the 16d sites. The $[B_2]X_4$ framework of the spinel is thus maintained throughout lithiation.

When derived from a lithium-deficient spinel, i.e. $Li_{0.94}V_2O_4$, a fraction of vanadium cations, initially in the tetrahedral 8a sites, migrate at an early stage of the lithiation to the octahedral 16c sites.

the 16c sites, with a B_{iso} factor arbitrarily fixed at 1.0 $Å^2$. The isotropic temperature factors of the vanadium and the oxide ions were refined, as were the anion position coordinates.

In the following cycle, the lithium ions were allowed to occupy both the tetrahedral 8a and the octahedral 16c sites, whereas the vanadium cations were distributed over the octahedral 16c and 16d sites. The total contents of lithium and vanadium ions were both fixed to 2.0, in accordance with the formula $Li_2V_2O_4$.

In the refined structure, which gave a reliability factor of 6.5%, 1.9(3) lithium ions are situated in the octahedral 16c sites, and 0.1(3) in the tetrahedral 8a sites. Although most of the vanadium ions, viz. 1.93(4), occupy the 16d sites, as in the spinel $Li[V_2]O_4$, a small fraction (0.07(4)) is found in the 16c sites. These values are in good agreement with the vanadium distribution obtained for $Li_{1.5}V_2O_4$, and confirm lithium-deficiency in the starting material, with a structure of the type $(Li_{0.93}V_{0.07})_{8a}[V_{1.93}\square_{0.07}]O_4$. The full structural parameters of $Li_2V_2O_4$ are listed in Table 6.7a, the observed and calculated ntensities in Table 6.7b.

This model indicates that, within experimental error, for the composition $Li_2V_2O_4$, all the lithium cations are situated in the octahedral 16c sites. The structure of $Li_2V_2O_4$ is thus a partially ordered rocksalt phase, where all the lithium cations are situated in the 16c sites (vacant in spinels) and the vanadium cations reside in the 16d sites. The $[B_2]X_4$ framework of the spinel is thus maintained throughout lithiation.

When derived from a lithium-deficient spinel, i.e. $Li_{0.94}V_2O_4$, a fraction of vanadium cations, initially in the tetrahedral 8a sites, migrate at an early stage of the lithiation to the octahedral 16c sites.

TABLE 6.7a

Structural parameters of $Li_{2.0}V_2O_4$

R = 6.5%

Space group: $Fd\bar{3}m$ (O_h^7) a = 8.291(1) Å

Atom	Position	x	y	z	B[Å^2]	n
Li^+	8a	0.125	0.125	0.125	1.0	0.1(3)
Li^+	16c	0.000	0.000	0.000	1.0	1.9(3)
V^{3+}	16c	0.000	0.000	0.000	0.4	0.07(4)
V^{3+}	16d	0.500	0.500	0.500	0.4(3)	1.93(4)
O^{2-}	32e	0.256(2)	0.256(2)	0.256(2)	2.0	4.0

TABLE 6.7b

Observed and calculated intensities for $Li_{2.0}V_2O_4$

hkl	I_{obs}	I_{calc}	hkl	I_{obs}	I_{calc}
111	477	484	551	44	32
311	230	210	711		
222	73	37	553	31	31
400	563	576	731		
331	54	62	800	32	32
511	76	79	751	43	49
333			555		
			662		
440	266	276	840	103	100
531	70	65	753	18	27
533	64	57	911		
622			842		
444	70	72			

6.5 ELECTROCHEMICAL CHARACTERISATION

6.5.1 Electrochemical curve

The electrochemical curve, showing the open-circuit-voltage (o.c.v.) versus the composition, x in $Li_{0.94+x}V_2O_4$, is given in Fig. 6.4.

This curve shows that lithium insertion into $Li_{0.94+x}V_2O_4$ proceeds in three stages. Initially, for $0<x\leq0.45$, the o.c.v. decreases slowly, from 2.37 V to 2.22 V (Stage I). This stage of the lithiation process can in turn be divided into two steps: up to $x \approx 0.3$ the drop in the o.c.v. value is very small (2.37 V to 2.32 V), whereas for $0.3<x\leq0.45$, the slope is slightly steeper. The initial gradual decrease indicates that very little energy is required during the first phase of the lithiation. In tne next step, for $0.45<x\leq1.10$, a more pronounced slope is observed; at $x=1.10$, the o.c.v. = 1.50 V (Stage II).

Both Stages I and II are single-phase reactions. Taking into account the lithium deficiency in the starting material, at $x=1.10$ the overall composition is $Li_2V_2O_4$. Beyond this composition, a voltage plateau is observed, indicating a multi-phase process (Stage III).

A mechanistic interpretation of the electrochemical curve will be given in section 6.6.

The theoretical energy density of the cell calculated from the electrochemical curve amounts to 348 Wh/kg (based on the cathode weight in the discharged state exclusively). Although this value is inferior to that of other vanadium oxides (e.g. 890 Wh/kg in the case of V_6O_{13} [86]), it only takes into account the energy obtainable from the system $LiV_2O_4 \rightarrow Li_2V_2O_4$; the complete system $Li_{1-x}V_2O_4 \rightarrow Li_{1+x}V_2O_4$ will be considered in chapter 7.

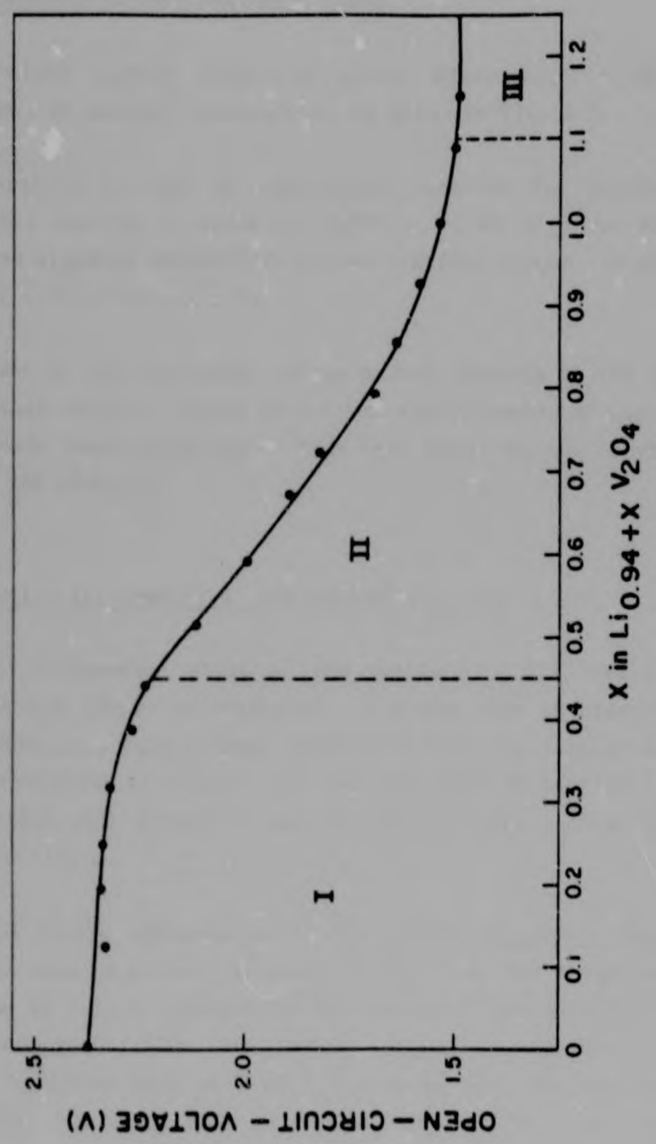

FIG. 6.4

Ambient temperature electrochemical curve of the cell $Li/LiClO_4$ 1M (P.C.)/$Li_{0.94}V_2O_4$

6.5.2 Constant current discharge curve

The constant current discharge curve, obtained at a rate of 20 $\mu A/cm^2$, at ambient temperature, is given in Fig. 6.5.

The operating voltage is practically constant for $0<x<0.7$ in $Li_{1+x}V_2O_4$, and has a value of 2.375 - 2.350 V. The voltage decreases steadily thereafter, in two distinct stages, to reach a value of 1.50 V for $x \approx 1.70$.

The extent of the discharge voltage plateau amounts to 70% of the theoretical capacity (based on a final stoichiometry of $Li_2V_2O_4$). The cathode capacity estimated from this curve amounts to approximately 109 mA-hr/g.

6.5.3 Cyclic voltammetry of the system $Li_{1+x}V_2O_4$

A cyclic voltammetry study of the system $Li_{1\pm x}V_2O_4$ was undertaken in the course of this work. For the sake of clarity and convenience, the full system, comprising both the lithiation and the delithiation of LiV_2O_4, will be described in Section 7.5.2. This section will therefore deal exclusively with lithium insertion into LiV_2O_4.

A typical cyclic voltammogram of the system $Li_{1+x}V_2O_4$, obtained at a scan rate of 1 mV/s, is shown in Fig. 6.6. The single reduction peak at 2.16 V, observed in the course of the cathodic scan, corresponds to the lithiation $LiV_2O_4 \rightarrow Li_2V_2O_4$. Upon scan reversal, an oxidation peak at 2.67 V indicates that the reaction is reversible. The large peak separation ($\Delta E_p \approx 0.51$ V) is typical of chemically reversible intercalation processes [85,100]. Figure 6.7 illustrates a cyclic voltammogram recorded at a slower scan rate (0.5 mV/s); it is similar to the one observed at 1 mV/s. The cathodic and anodic peak potentials are shifted closer to

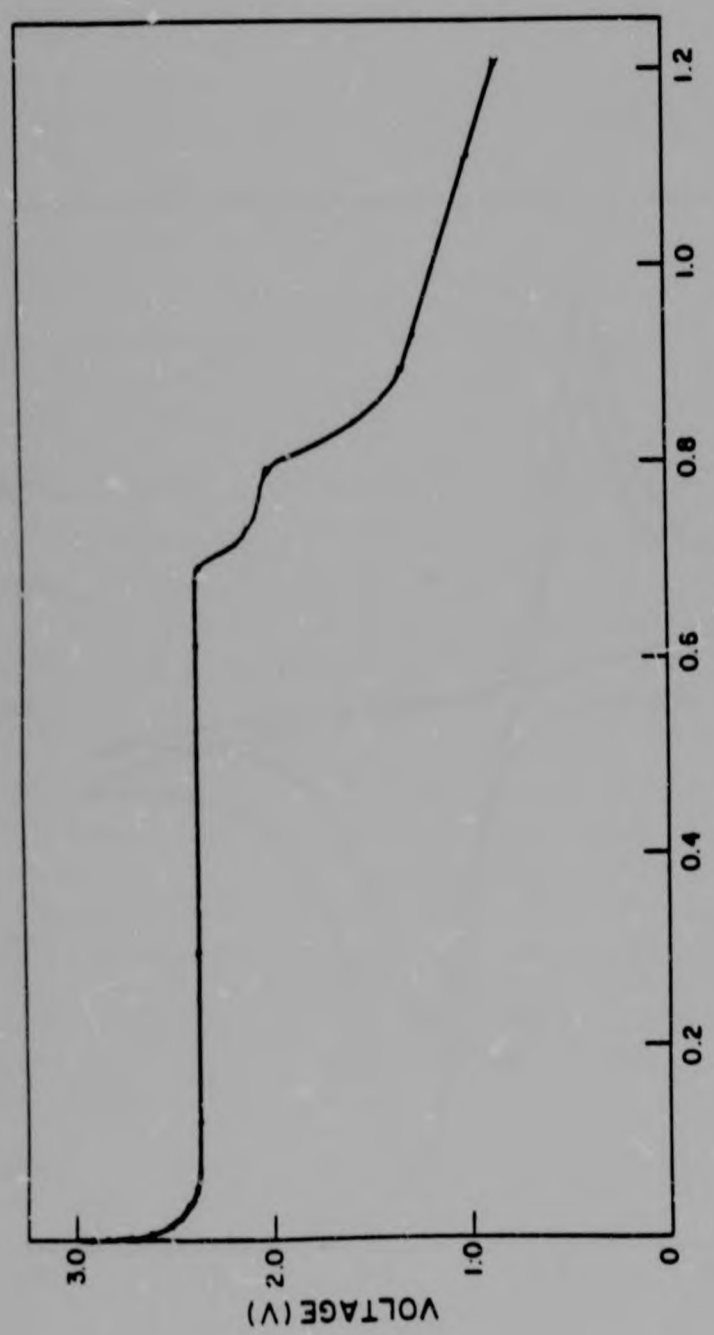

FIG. 6.5

Constant current discharge curve of the cell $Li/LiClO_4$ 1M (P.C.)/$Li_{0.98}V_2O_4$ at 25 °C (20 μA, 10 mg LiV_2O_4)

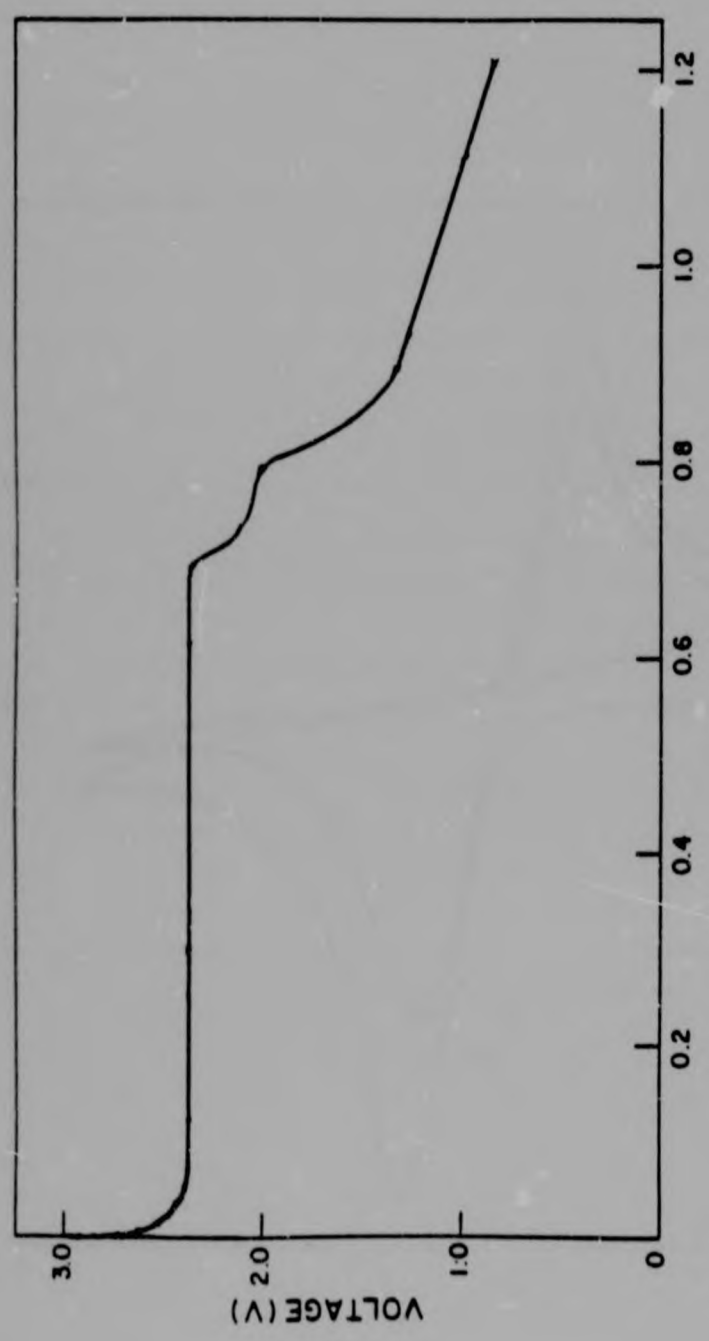

FIG. 6.5

Constant current discharge curve of the cell Li/$LiClO_4$ 1M (P.C.)/$Li_{0.98}V_2O_4$ at 25 °C (20 μA, 10 mg LiV_2O_4)

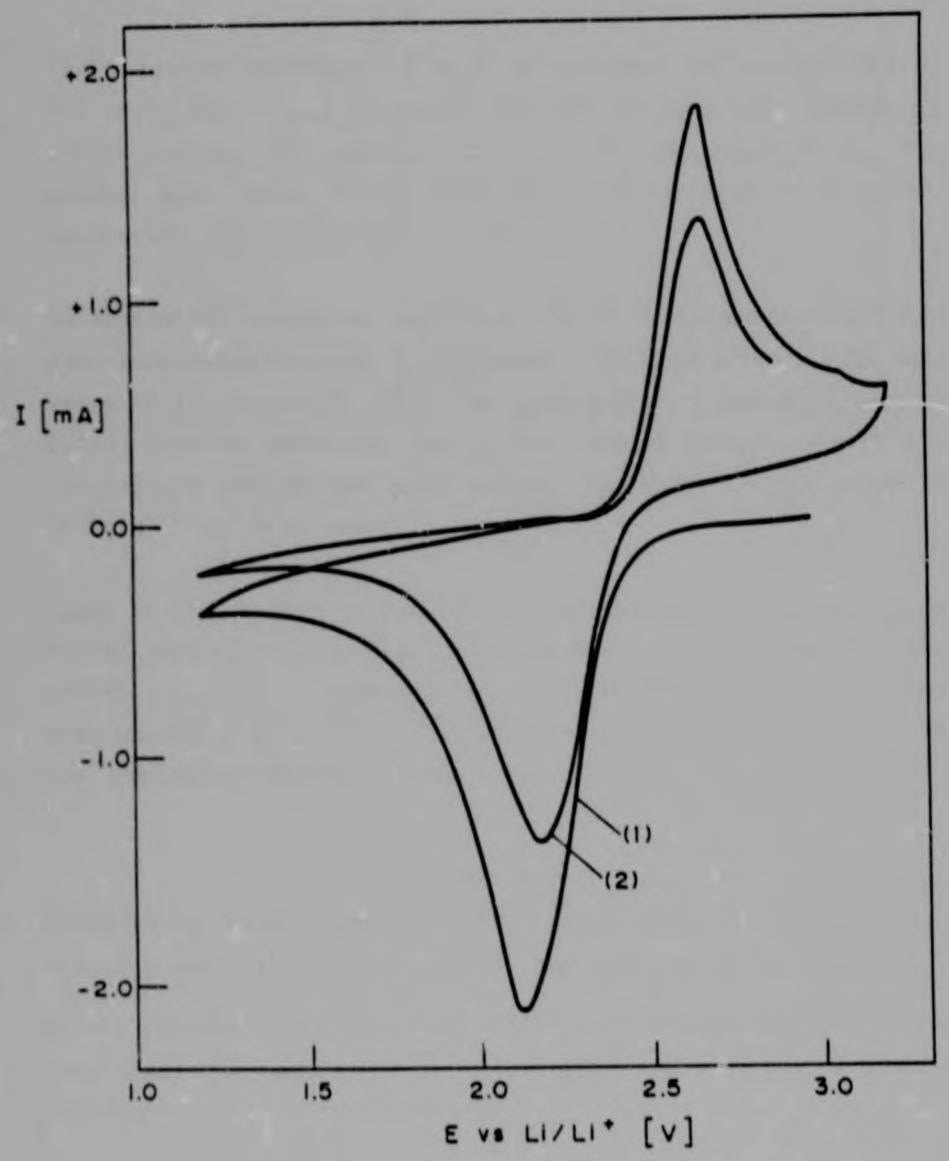

FIG. 6.6
Cyclic voltammogram of the system $Li_{1+x}V_2O_4$ ($0<x<1$)
(v = 1 mV/sec)

each other, and have the values of 2.25 V and 2.61 V respectively. At a scan rate of 0.1 mV/s this phenomenon is more accentuated, with a reduction at 2.32 V and an oxidation at 2.53 V (Fig. 7.11).

The reduction potential of 2.32 V, obtained at a scan rate of 0.1 mV/s, is in good agreement with the galvanostatic discharge-curve plateau (cf section 6.5.2). The decrease of ΔE_p for slower scan rates (Table 6.8) is characteristic of a quasi-reversible electrochemical process.

Intercalation reactions are often found to be quasi-reversible when investigated by cyclic voltammetry with relatively fast scan rates (0.1 - 1 mV/s). As it was previously discussed in section 2.5.3, this is generally due to the slow diffusion rate of the intercalate through the host lattice (typically in the order of 10^{-8}-10^{-12} cm^2/s or less).

Owing to the absence of complete electrochemical reversibility, a formal reduction potential ($E^{0'}$) cannot be calculated for the system $Li_{1+x}V_2O_4$. However, it is interesting to note that the mean potential $\bar{E}$ $\left(= \frac{E_{pa} + E_{pc}}{2}\right)$ has the value of 2.43(1) V for all the scan rates observed (Table 6.8).

TABLE 6.8

Cathodic and anodic peak potentials (E_{pc}, E_{pa}), ΔE_p ($= E_{pa} - E_{pc}$) and mean potential $\bar{E}$ $\left(= \frac{E_{pa} + E_{pc}}{2}\right)$ for different scan rates (v)

v [mV/s]	E_{pc} [V]	E_{pa} [V]	ΔE [V]	$\bar{E}$ [V]
1.0	2.16	2.67	0.51	2.42
0.5	2.25	2.61	0.36	2.43
0.1	2.32	2.53	0.21	2.43

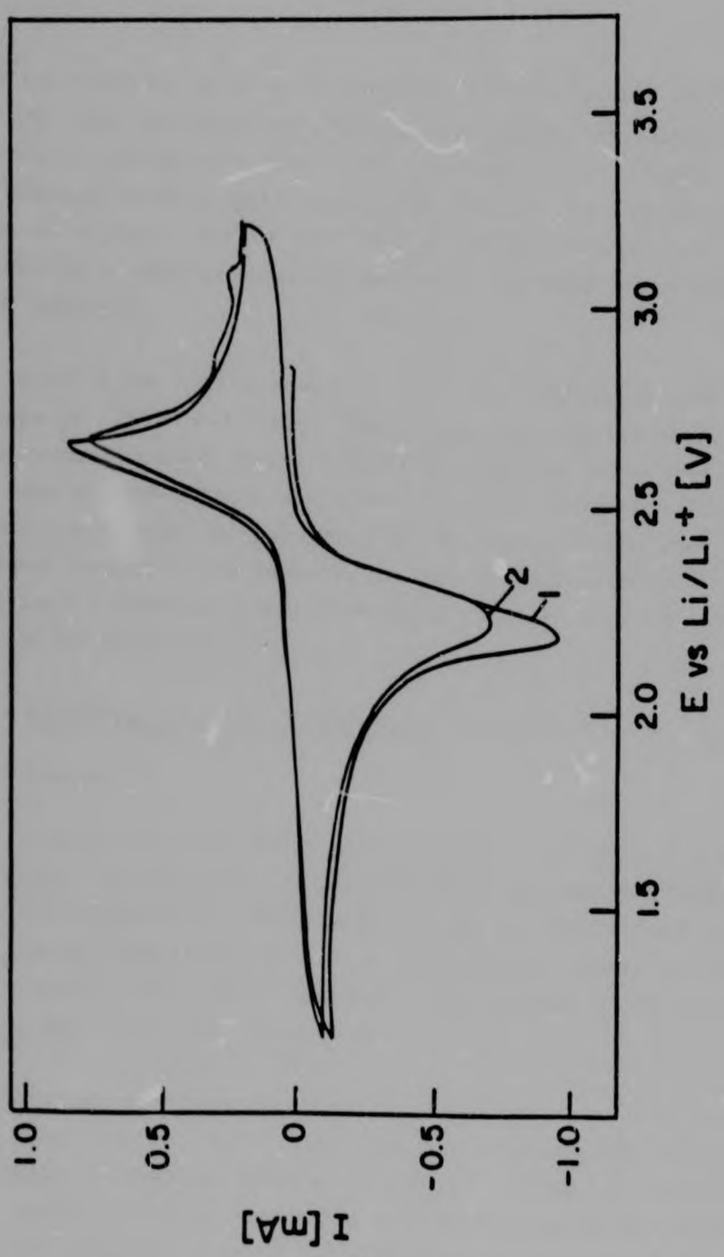

FIG. 6.7

Cyclic voltammogram of the system $Li_{1+x}V_2O_4$ ($0<x<1$)

(v = 0.5 mV/sec)

For approximately equal electrode areas (~0.5 cm^2), the intensity of the peak decreases with slower scan rates, as expected in diffusion-limited processes. The intensity of the reverse peak is observed to be slightly lower than that of the forward scan: this is probably due to the loss of active material from the electrode, a commonly observed feature in the study of intercalation compounds.

The broad shape of the peaks is a further indication that the process is diffusion-limited. Theoretical calculations predict a very gradual current decay, resulting in a very broad peak, in the case of semi-infinite diffusion [115,116]. Diffusion through a solid electrode is considered to be semi-infinite when the distance covered by the inserted ion during the time-scale of the experiment is several orders of magnitude smaller than the thickness of the electrode [115].

6.5.4 Li$^+$ diffusion rates in the system $Li_{1+x}V_2O_4$ $(0<x<1)$

a) Results

Lithium diffusion rates were determined in samples where $0<x<1$ in $Li_{1+x}V_2O_4$ (Table 6.9). This was possible because lithium insertion into LiV_2O_4 follows two single-phase processes throughout the entire compositional range, in contrast to many other vanadium oxide systems where multiphase regions are observed [83].

Lithium diffusion in the spinel $Li[V_2]O_4$ is relatively slow, viz. $\tilde{D} = 4.10^{-10}$ cm^2/sec, but increases with lithiation, to reach a value of $\tilde{D} = 6.10^{-8}$ cm^2/sec in the end-product $Li_2[V_2]O_4$, which has an ordered rocksalt structure. The variation of $\log \tilde{D}$ as a function of lithium content is depicted in Fig. 6.8: a linear increase is observed between $0<x<0.55$. Beyond $x\approx0.55$, there is a discontinuity in the plot, after which $\log \tilde{D}$ increases less rapidly with lithium content.

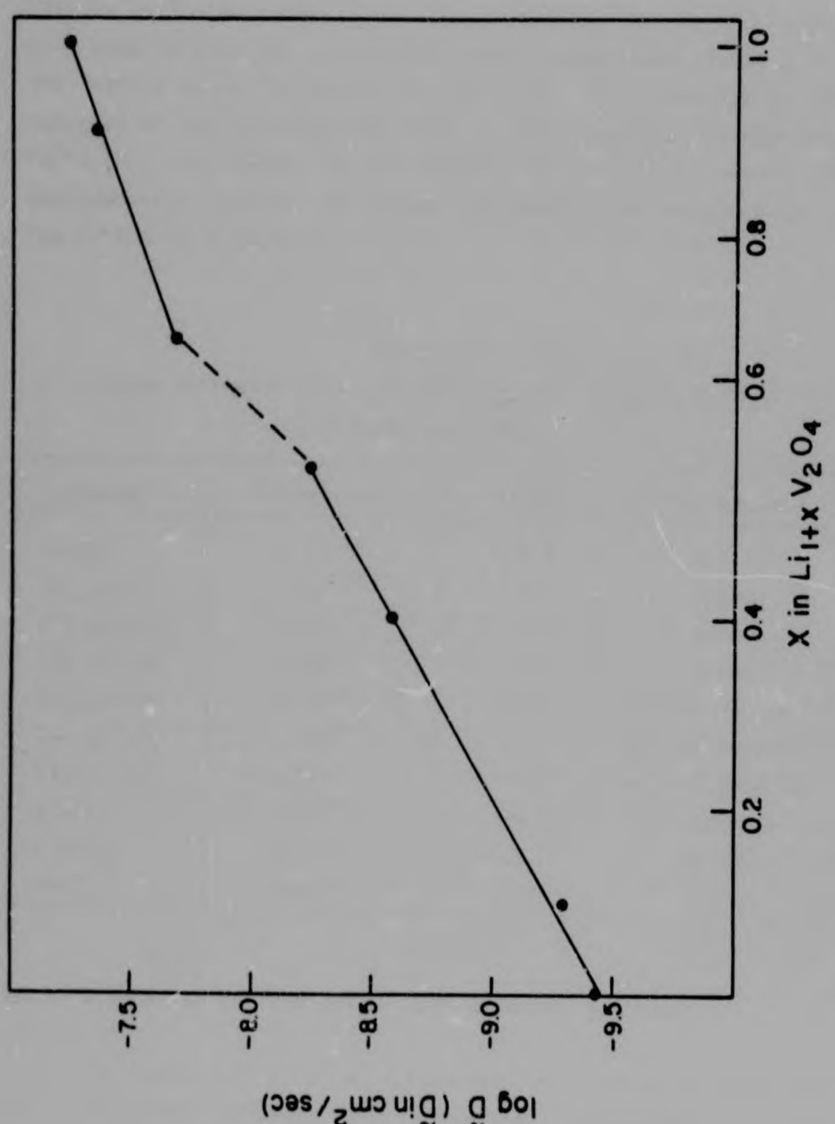

FIG. 6.8
Variation of $\tilde{D}$ as a function of lithium content in $Li_{1+x}V_2O_4$ ($0<x<1$)

Lithium diffusion rates in two other spinels, $LiMn_2O_4$ and Fe_3O_4, were also determined, in order to draw a comparison (Table 6.9). The lithium spinel $Li[Mn_2]O_4$ was selected, as it belongs to the category of the $Li[M_2]O_4$ (M = Ti, V, Mn) spinels. Magnetite, $Fe[Fe_2]O_4$, was chosen as an example of a spinel capable of accommodating lithium, in which the A-site is occupied by a transition-metal cation.

TABLE 6.9

Lithium diffusion rates ($\tilde{D}$) in $Li_{1+x}V_2O_4$ ($0<x<1$), $LiVO_2$, $LiMn_2O_4$ and Fe_3O_4

Compound	$\tilde{D}$ [cm^2/sec]	log $\tilde{D}$	Structure
LiV_2O_4	4.10^{-10}	- 9.4	spinel
$Li_{1.10}V_2O_4$	5.10^{-10}	- 9.3	spinel
$Li_{1.40}V_2O_4$	3.10^{-9}	- 8.6	spinel
$Li_{1.56}V_2O_4$	6.10^{-9}	- 8.2	spinel
$Li_{1.69}V_2O_4$	2.10^{-8}	- 7.7	"defect rocksalt"
$Li_{1.90}V_2O_4$	1.10^{-8}	- 7.9	"defect rocksalt"
$Li_{2.0}V_2O_4$	6.10^{-8}	- 7.2	"ordered rocksalt"
$LiVO_2$	5.10^{-9}	- 8.3	layered
$LiMn_2O_4$	1.10^{-11}	-11.0	spinel
Fe_3O_4	4.10^{-11}	-10.4	spinel

b) Discussion and comparison with selected compounds

The variation of $\tilde{D}$ as a function of lithium content in $Li_{1+x}V_2O_4$ reflects the structural modifications which occur during lithiation (Section 6.4).

The discontinuity in the plot log $\tilde{D} = f(x)$ coincides with with the structural transformation from spinel to a partially ordered rocksalt structure, observed by powder X-ray

diffraction. This structural change, which is provoked by the migration of Li^+ ions from the A-sites to the 16c octahedra, is also evidenced by the sudden increase of the cell constant (Fig. 6.1) and the slope change in the electrochemical curve (Fig. 6.4). The cell volume expansion may be correlated to the electronic conductivity mechanism, which changes from metallic to semiconducting in the same compositional range [165]: the localised vanadium 3d electrons induce the cell dilatation.

The increase of $\tilde{D}$ with lithiation can be correlated to the relative energies of the 8a and 16c sites and to the activation energy (E_a) between them.

In the spinel structure, the 8a tetrahedra, which contain the lithium ions, have the lowest energy, since they are situated furthest from the B-sites (Fig. 6.9a). In the $Li_2[V_2]O_4$ rocksalt phase, the 16c octahedra are of lower energy; these sites are therefore filled with lithium (Fig. 6.9b). Simultaneous occupation of the face-sharing 8a tetrahedra and 16c octahedra at this composition is energetically unfavourable because of the short 8a-16c intersite distance (1.78 Å). The $\tilde{D}$ values obtained would therefore indicate that the activation energy barrier between the 8a tetrahedra and the 16c octahedra is higher in the spinel $Li[V_2]O_4$ than in the rocksalt phase $Li_2[V_2]O_4$.

An intermediate situation is observed in the partially lithiated spinel $Li_{1.5}[V_2]O_4$, in which the 8a and 16c sites are simultaneously occupied (cf section 6.4.1). Despite the fact that the 8a and 16c site energies must be fairly similar, $\tilde{D}$ indicates that E_a is lower than in the spinel, but higher than in the rocksalt phase.

Lithium-ion diffusion in $Li[Mn_2]O_4$ is 1.10^{-11} cm^2/sec and is considerably slower than in the isostructural vanadium spinel. The difference in $\tilde{D}$ values between the two com-

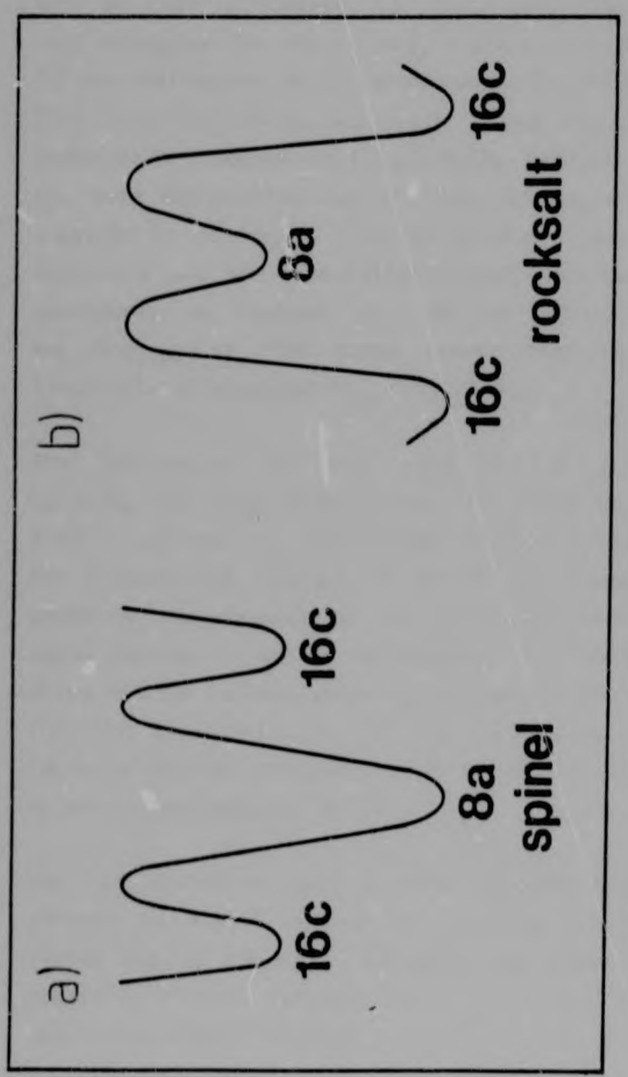

FIG. 6.9

Schematic representation of the site energy differences between the 8a and 16c sites in spinel and rocksalt

pounds can be attributed partly to the difference in electronic conductivity, as $Li[V_2]O_4$ is a metallic conductor [167], and $Li[Mn_2]O_4$ is a semiconductor [168] (E_a = 0.44 eV [169]); however, $Li_{1+x}V_2O_4$ also becomes a polaronic conductor for x>0.4 [165], where $\tilde{D}$ is high. The Jahn-Teller distortion, which accompanies the $Mn^{4+} \rightarrow Mn^{3+}$ reduction upon lithiation, and which lowers the symmetry from cubic to tetragonal in $Li_{1+x}[Mn_2]O_4$ (x>0.1), is probably the main explanation for the low lithium diffusion rate observed in $Li[Mn_2]O_4$. The difference in electronic conductivity and the Jahn-Teller effect have been suggested previously as reasons why the Na^+ diffusion rate in $Na_{0.7}MnO_{2.25}$ is ~200 times slower than it is in the isostructural compound $Na_{0.7}CoO_2$ [170].

The lithium-ion diffusion rate in the lithium spinel $Li[V_2]O_4$ is also higher than in $Fe[Fe_2]O_4$, where $\tilde{D} = 4.10^{-11}$ cm^2/sec. In the latter, lithium diffusion through the interstitial channels of the $[B_2]X_4$ framework is hampered by the presence of the relatively heavy transition metal cations in the 8a tetrahedra. The steric hindrance which reduces Li^+-ion mobility is probably the major reason for the irreversibility of the lithiation reaction of Fe_3O_4, which has been observed by chemical cycling [73] and by cyclic voltammetry [140].

The Li^+ diffusion rate in the layered compound $LiVO_2$ amounts to 5.10^{-9} cm^2/sec (cf section 4.5.3), which is faster than in the spinel $Li[V_2]O_4$, but slower than in the partially ordered rocksalt phase $Li_2[V_2]O_4$ (which has the same stoichiometry as $LiVO_2$).

6.6 REACTION MECHANISM

The combined structural and electrochemical data suggest the following mechanism for lithium insertion into the spinel $Li_{0.94}V_2O_4$.

Initially a critical concentration (x_c) of lithium is intercalated into the vacant octahedral 16c sites of the spinel structure:

$$(Li_{0.94}V_{0.06})8a\ [V_{1.94}\square_{0.06}]16d O_4$$

$$\downarrow\ x_c Li$$

$$(Li_{0.94}V_{0.06})8a\ \{Li_{x_c}\}16c\ [V_{1.94}\square_{0.06}]16d O_4$$

As discussed in preceding chapters, tri- or tetravalent vanadium cations are not usually stable in a tetrahedral coordination. It is therefore likely that vanadium cations in the tetrahedral 8a sites are pentavalent, and are reduced at an early stage of the lithiation process: they would then become unstable in the 8a sites.

Furthermore, the electrostatic interactions between a small number of inserted lithium ions in the 16c sites and the pentavalent vanadium cations in the neighbouring face-sharing 8a sites are probably sufficiently strong to displace the vanadium ions from the 8a to the 16c sites, particularly in view of the very short inter-site distance of 1.78 Å.

At an early stage of the reaction, therefore, the vanadium cations migrate to the 16c sites; lithium insertion then proceeds smoothly up to the composition $Li_{1.5}V_2O_4$ (Stage I):

$$(Li_{0.94}V_{0.06})8a\ \{Li_{x_c}\}16c\ [V_{1.94}\square_{0.06}]16d O_4$$

$$\downarrow$$

$$(Li_{0.94})8a\ \{Li_{x_c}V_{0.06}\}16c\ [V_{1.94}\square_{0.06}]16d O_4$$

$$\downarrow\ (0.56 - x_c)Li$$

$$(Li_{0.94})8a\ \{Li_{0.56}V_{0.06}\}16c\ [V_{1.94}\square_{0.06}]16d O_4$$

Up to the stoichiometry $Li_{1.5}V_2O_4$, the lithium cations, initially present in the parent compound LiV_2O_4, remain in the 8a sites: the electrostatic interaction between lithium cations in the face-sharing 8a and 16c sites is not strong enough to cause the former to migrate. Up to this composition, the open-circuit voltage decreases slowly (Fig. 6.4), and $\log \tilde{D} = f(x)$ increases linearly (Fig. 6.8). Similarly, only a slight cell expansion is observed (Fig. 6.1) whilst the relative intersities of individual reflections are scarcely changed.

As lithiation proceeds beyond $Li_{1.5}V_2O_4$, a second process is observed on the electrochemical curve. The lithium-ion diffusion rate suddenly increases, provoking a discontinuity in the $\log \tilde{D} = f(x)$ plot at $x>0.55$ (Fig. 6.8). From a structural point of view, the cell constant also increases, and relative peak intensities change.

As the octahedral 16c sites are progressively filled, the interactions between the original Li^+ ions in the 8a sites and the inserted Li^+ ions increase, causing the former to transfer from the 8a sites to the 16c octahedra. Lithiation then continues up to the end-composition $Li_2V_2O_4$ (Stage II):

$$(Li_{0.94})_{8a}\,\{Li_{0.56}\ V_{0.06}\}_{16c}\,[V_{1.94}\ \square_{0.06}]_{16d}\ O_4$$

$$\downarrow\ 0.5\ Li$$

$$(Li_{0.06})_{8a}\,\{Li_{1.94}\ V_{0.06}\}_{16c}\,[V_{1.94}\ \square_{0.06}]_{16d}\ O_4$$

The end-product $Li_2V_2O_4$ has a partially ordered rocksalt structure. Most of the lithium ions and a small fraction of the vanadium cations (0.07(4)), initially situated in the 8a sites, reside in the octahedral 16c sites.

Although the structural refinement indicates the presence of 0.1(3) lithium cations in the 8a sites, the exact location of these cannot be determined unequivocally, due to the low X-ray scattering power of lithium ions. An alternative to the structure given above would be the rocksalt phase:

$$\{Li_{0.94}\ V_{0.06}\}_{16c}\ [Li_{0.06}\ V_{1.94}]_{16d}\ O_4$$

In this model, which gave an R factor of 7.0%, all the octahedral sites are filled. This would require the migration of lithium cations along the pathway 8a → 16c → 48f → 16d.

The occupancies of the vanadium cations in the 16c sites for $Li_{1.5}V_2O_4$ and $Li_{2.0}V_2O_4$, viz. 0.08(4) and 0.07(4) respectively, are in good agreement with one another. These values confirm that the starting material is lithium-deficient (i.e. $Li_{0.94}V_2O_4$) as found by atomic absorption spectrometry and that the vacancies thus created on the 8a sites are occupied by vanadium.

The products of the electrochemical reaction for $x > 1.10$ (Stage III) could not be identified. Chemically, using n-BuLi, it was not possible to insert lithium beyond the composition $Li_2V_2O_4$.

In summary, lithium diffuses into LiV_2O_4 through the three-dimensional network of inter-connected 16c-8a-16c channels of the spinel $[B_2]X_4$ sub-lattice. Structural data shows that the end-product $Li_2V_2O_4$ has a partially ordered rocksalt structure, where the lithium cations occupy the 16c octahedral positions, whilst the spinel $[B_2]X_4$ framework remains intact. The cyclic voltammograms of the system $Li_{1+x}V_2O_4$ for the range $0<x<1$ show that lithiation is fully reversible and that the same process is repeated in the course of the second (and subsequent) cycles. This constitutes further evidence that the host structure remains intact throughout the entire lithiation and delithiation process.

6.7 CONCLUSIONS

Topochemical lithium insertion into the spinel $Li_{\sim 1.0}V_2O_4$ is possible and leads to the formation of $Li_2V_2O_4$. It is interesting to compare the lithiation process of LiV_2O_4 with the isostructural spinels $LiMn_2O_4$ and $LiTi_2O_4$. Both the structural and the electrochemical aspects will be discussed.

From a structural point of view, the lithiated spinels $Li_2Ti_2O_4$, $Li_2V_2O_4$ and $Li_2Mn_2O_4$ are very similar. As in the case of other oxide and sulphide spinels, lithium is initially inserted into the vacant octahedral 16c sites. The lithiation process can be expressed as follows:

$$(Li)_{8a}[M_2]_{16d}O_4 \xrightarrow{xLi} (Li)_{8a}\{Li_x\}_{16c}[M_2]_{16d}O_4$$

$$\downarrow 1-x\ Li$$

$$(Li_{1-y})_{8a}\{Li_{1+y}\}_{16c}[M_2]_{16d}O_4 \quad (0<y\leq 1)$$

The end-products $Li_2M_2O_4$ (M = V,Ti,Mn) differ slightly: as in the case of $Li_2V_2O_4$, $Li_2Ti_2O_4$ has a partially ordered rocksalt structure ($\{Li_2\}_{16c}[Ti_2]_{16d}O_4$) [164]. In $Li_2Mn_2O_4$, however, the lithium cations were found to be almost randomly distributed over the tetrahedral 8a and the octahedral 16c sites [33,163]. Simultaneous occupation of the face-sharing tetrahedra and octahedra is also observed in the case of the intermediate compound $Li_{1.5}V_2O_4$.

Although these findings may appear surprising, particularly in view of the very short inter-site distance (1.78 Å) between the 8a and 16c positions, it must be stressed that 50% and 33% of the combined 8a and 16c sites in $Li_{1.5}V_2O_4$ and $Li_2Mn_2O_4$

respectively remain vacant. Furthermore, the structures obtained in the course of the X-ray diffraction study represent a statistical representation of the location of the atoms. Due to the presence of vacant sites, it is therefore possible that, at any given time, only a few cation pairs within the crystal occupy face-sharing sites. Cation occupation of face-sharing sites has previously been reported in the case of $Ni_{2.44}Ti_{0.77}O_4$, a spinel with an excess of cations, for which the structure $(Ti_{0.77})_{8a}\{Ni_{0.44}\}_{16c}[Ni_2]_{16d}O_4$ has been proposed [171].

Contrary to $LiMn_2O_4$, it is not possible to insert lithium into LiV_2O_4 beyond the composition $Li_2V_2O_4$. Lithiation beyond $Li_2Mn_2O_4$ results in a layered structure with the composition Li_2MnO_2. This compound has a hexagonally close-packed array of anions, where the Mn^{2+} ions are situated in octahedral sites in alternate layers, and the Li^+ ions are located in edge-shared tetrahedra in adjacent layers; in Li_2MnO_2 the Li^+-Li^+ interionic distance is 2.1 A [172].

The electrochemical characteristics of LiV_2O_4 compare favourably with the isostructural compounds $LiMn_2O_4$ and $LiTi_2O_4$.

For consistency, galvanostatic discharge curves of all three compounds LiM_2O_4 (M = Ti,V,Mn) were recorded, using an identical cell assembly (cf Fig. 6.10). The discharge curve obtained for $LiTi_2O_4$ in this work is in excellent agreement with Murphy et al. [78]. Although the discharge plateau of $LiMn_2O_4$ is very long compared to $LiTi_2O_4$ and LiV_2O_4, the operating voltage is extremely low (viz. 0.30 V), indicating excessively high polarisation effects, largely due to very low Li^+ mobility. Whilst the discharge plateaux of LiV_2O_4 and $LiTi_2O_4$ are of a similar length, the operating voltage of LiV_2O_4 (viz. 2.36 V) is considerably higher than that of $LiTi_2O_4$ (1.33 V). The practical energy density of the system $Li_{1+x}V_2O_4$ $(0<x<1)$ is therefore considerably greater than that of the Mn and Ti analogues.

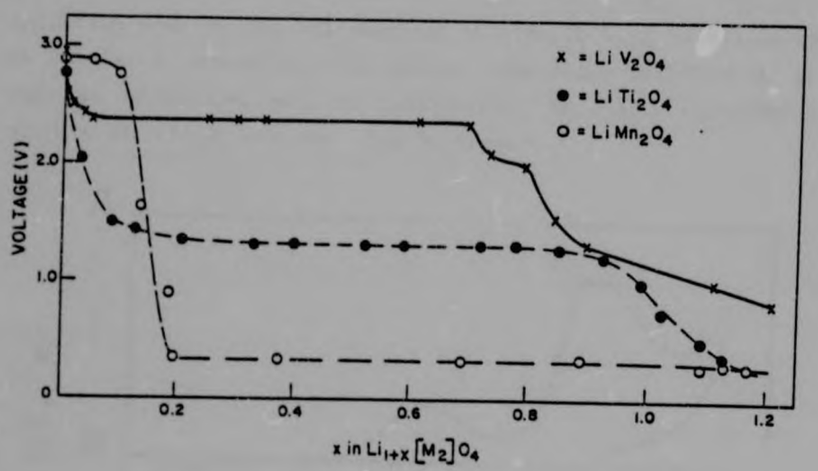

FIG. 6.10
Constant current discharge curves of the cells $Li/LiClO_4$ 1M (P.C.)/$Li[M_2]O_4$) (M = Ti, V, Mn) (20 $\mu A/cm^2$)

The discontinuity and slope changes observed in the case of $Li_{1+x}V_2O_4$ for $0.75<x<0.9$ are possibly due to a sudden structural change, such as the migration of Li^+ ions from the tetrahedral 8a to the octahedral 16c sites. Discontinuities in the discharge curve are often observed in intercalation systems, as for example in the vanadium compounds $Li_xV_6O_{13}$ [82] and $Li_{1+x}V_3O_8$ [95].

The cyclic voltammetric behaviour of $Li_{1+x}V_2O_4$ and $Li_{1+x}Mn_2O_4$ is very similar. Hunter and Tudron [100] report a cyclic voltammogram of $LiMn_2O_4$, obtained at a scan rate of 1 mV/s (Fig. 6.11). A reduction peak at 2.60 V and a corresponding oxidation peak at

3.42 V are observed. The general appearance of the peaks and the peak separation (ΔE_p = 0.82 V) indicate a diffusion-controlled process similar to the system $Li_{1+x}V_2O_4$ (Fig. 6.6). The next oxidation peak in the voltammogram of $LiMn_2O_4$ will be discussed in Chapter 7, where the full system, comprising delithiation as well as lithiation, will be considered. No cyclic voltammetry studies of $LiTi_2O_4$ are available at present.

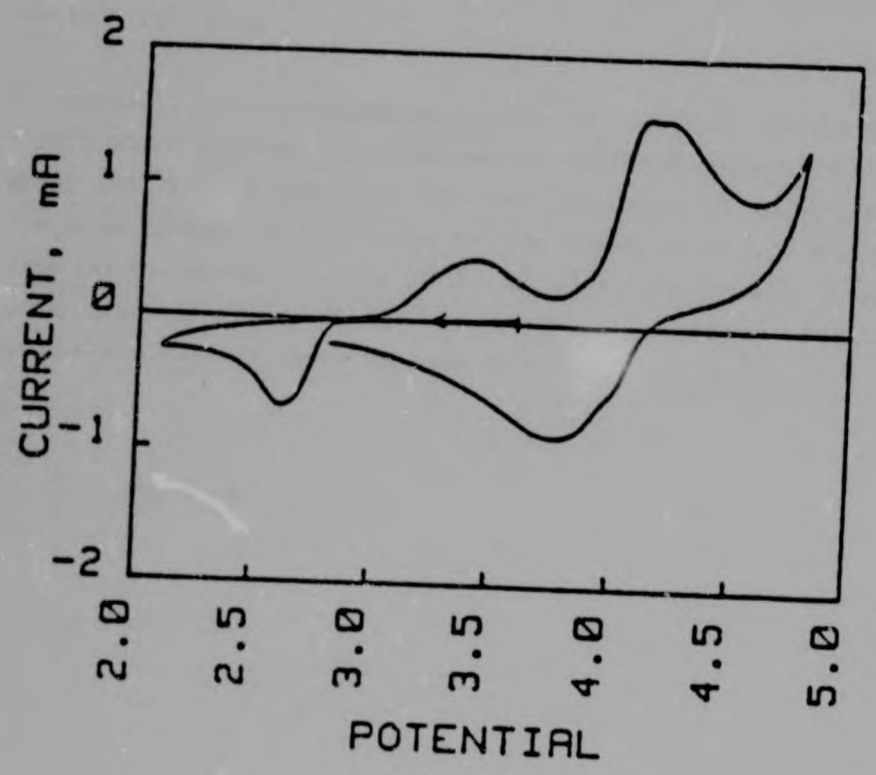

FIG. 6.11
Cyclic voltammogram of $LiMn_2O_4$ (v = 1 mV/sec) (from ref.100)

Lithium-ion diffusion in LiV_2O_4 is ~40 times faster than in $LiMn_2O_4$. The possible reasons for this were discussed in section 6.5.4b. The low diffusion rate measured in $LiMn_2O_4$ explains the high polarisation effect observed in the galvanostatic discharge curve.

The open-circuit voltage curve of $Li_{1+x}V_2O_4$ differs markedly from that of $Li_{1+x}Mn_2O_4$. The latter shows a voltage plateau for $0.1<x<1.8$, and a sharp potential drop between $0.8<x<1.0$ [33]. The voltage plateau is indicative of a two-phase process. X-ray diffraction patterns of $Li_{1+x}Mn_2O_4$ samples confirm the coexistence of a cubic and a tetragonal phase [33]. The latter arises from a cooperative Jahn-Teller distortion, due to the presence of the Mn^{3+} (d^4) ions.

In contrast, the electrochemical curve of $Li_{1+x}V_2O_4$ reveals two single-phase regions, characterised by different slopes, during which the cubic symmetry of the host structure is maintained. The slope change is attributed to the migration of Li^+ cations from the tetrahedral A sites of the spinel to the formerly vacant octahedral 16c sites. Preliminary data [173] suggests a similar single-phase behaviour in the case of $Li_{1+x}Ti_2O_4$.

CHAPTER 7

LITHIUM EXTRACTION FROM LiV_2O_4

7.1 INTRODUCTION

Lithium insertion into the spinels $Li[M_2]O_4$ (M = Mn, Ti, V) has been discussed in Chapter 6. Lithium extraction from these spinels is of interest as it enhances the capacity of the $Li[M_2]O_4$ working electrode of a battery.

The delithiation of $LiMn_2O_4$, which has been studied in depth [74-76, 163] leads to the formation of λ-MnO_2, a novel form of manganese dioxide, with the spinel $[B_2]X_4$-framework structure. Delithiation of $LiTi_2O_4$ is reported to lead to a poorly crystalline compound with a disordered defect rocksalt structure, similar to fully delithiated $LiVO_2$ [77, 78].

In this chapter, lithium extraction from LiV_2O_4 will be studied from a structural and an electrochemical point of view.

7.2 EXPERIMENTAL

Lithium was extracted chemically and electrochemically from $Li_{0.98}V_2O_4$ and $Li_{0.95}V_2O_4$ samples, prepared by the route described in Chapter 5.

Chemical delithiation was carried out using a 0.125 M solution of Br_2 in chloroform, as described in Section 3.2.1. Reaction mixtures were stored at room temperature in darkness for 5-10 days. Lithium was extracted electrochemically at a constant current density of 20 $\mu A/cm^2$ in a two-electrode cell of the type:

$$LiV_2O_4 \;/\; LiClO_4\ 1M\ (P.C.)\;/\; LiMn_2O_4$$

Open-circuit voltages were recorded intermittently after equilibration times of up to 72 hours.

Cyclic voltammetry experiments were carried out according to the method described in Section 3.3.2.

7.3 RESULTS

Several samples with a range of compositions of $0<x<0.77$ in $Li_{1-x}V_2O_4$ were prepared by chemical oxidation.

Lithium extraction at ambient temperature proceeds relatively slowly: reaction times of several days using excess quantities of bromine were required to obtain maximum delithiation, i.e. a compound with the stoichiometry $Li_{0.23}V_2O_4$.

The powder X-ray diffraction patterns of materials with various compositions were examined (Table 7.1). Compounds with a high lithium content ($0<x<0.34$ in $Li_{1-x}V_2O_4$) were single-phase, and could be indexed to the cubic space-group Fd3m. The relative intensities of the reflections were unchanged with respect to the starting material $Li_{\sim 1.0}V_2O_4$. A typical X-ray pattern in this range of compositions is shown in Fig. 7.2. The cell constant decreased as a linear function of the composition, as shown in Fig. 7.1, reaching a value of $a = 8.213(2)$ Å for $Li_{0.66}V_2O_4$.

X-ray patterns of $Li_{1-x}V_2O_4$ samples with $0.34<x<0.72$ differed, depending on the starting material's lithium content.

Samples obtained from LiV_2O_4 and from slightly lithium-deficient spinels (e.g. $Li_{0.98}V_2O_4$) remain cubic. A contraction of the cell constant is observed with decreasing lithium content (cf Table 7.1).

In contrast, samples derived from spinels with a lower initial lithium concentration (e.g. $Li_{0.95}V_2O_4$) indicated the presence

of two phases, viz. a cubic and a trigonal phase (Fig. 7.3). In these samples, the trigonal phase predominated for low lithium content (Fig. 7.4). The cell constants are listed in Table 7.1. In all the extensively delithiated samples ($x \approx 0.7$ in $Li_{1-x}V_2O_4$) fairly sharp changes in the relative intensities of the reflections were observed (Figs 7.3 and 7.4).

TABLE 7.1

Structural data for a few samples of $Li_{1-x}V_2O_4$

Stoichiometry	Starting material	Symmetry of end-product	Cell constants [Å]
$Li_{0.85}V_2O_4$	$Li_{0.98}V_2O_4$	cubic	a = 8.228(1)
$Li_{0.72}V_2O_4$	"	cubic	a = 8.220(2)
$Li_{0.66}V_2O_4$	"	cubic	a = 8.213(2)
$Li_{0.55}V_2O_4$	"	cubic*	a = 8.209(2)
$Li_{0.46}V_2O_4$	"	cubic**	a = 8.212(3)
$Li_{0.45}V_2O_4$	$Li_{0.95}V_2O_4$	cubic +	a = 8.203(3)
		trigonal	a = 2.887(1)
			c = 14.20(1)
$Li_{0.43}V_2O_4$	"	cubic +	a = 8.206(2)
		trigonal	a = 2.886(1)
			c = 14.20(1)
$Li_{0.34}V_2O_4$	"	cubic +	a = 8.203(3)
		trigonal	a = 2.886(1)
			c = 14.206(9)
$Li_{0.27}V_2O_4$	$Li_{0.95}V_2O_4$	cubic +	a = 8.200(3)
		trigonal	a = 2.885(1)
			c = 14.17(1)
$Li_{0.28}V_2O_4$	$Li_{\sim 1.0}V_2O_4$	cubic	a = 8.151(3)
$Li_{0.25}V_2O_4$	$Li_{\sim 1.0}V_2O_4$	cubic	a = 8.154(3)
$Li_{0.23}V_2O_4$	$Li_{\sim 1.0}V_2O_4$	cubic	a = 8.158(2)

* Predominantly cubic; trigonal phase reflections present, but not sufficiently sharp to be indexed.

** Predominantly cubic; relative intensities begin to change.

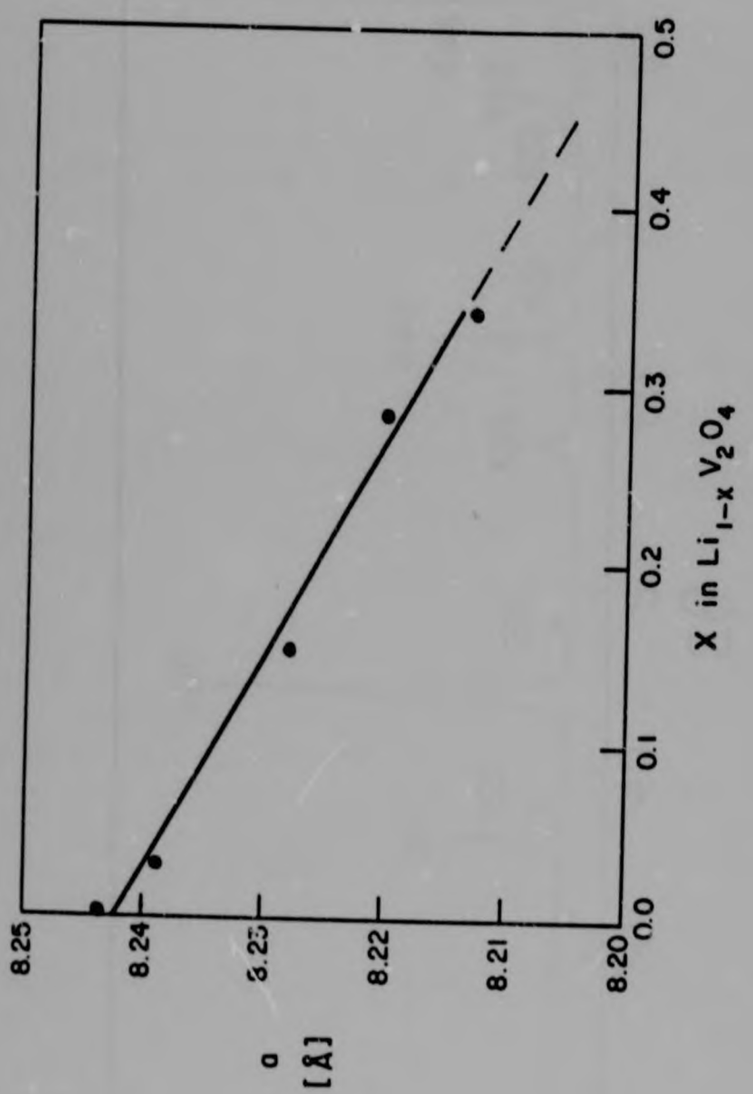

FIG. 7.1
Variation of the lattice parameter "a" with composition, x, in $Li_{1-x}V_2O_4$

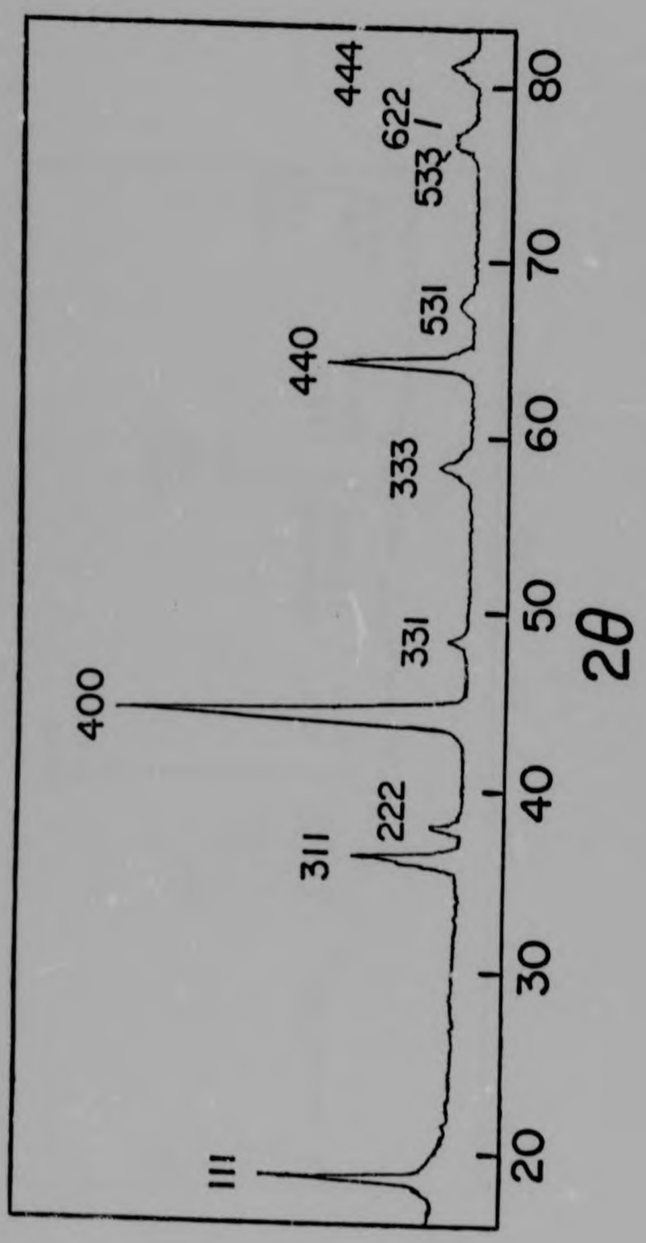

FIG. 7.2
X-ray diffraction pattern of $Li_{0.72}V_2O_4$

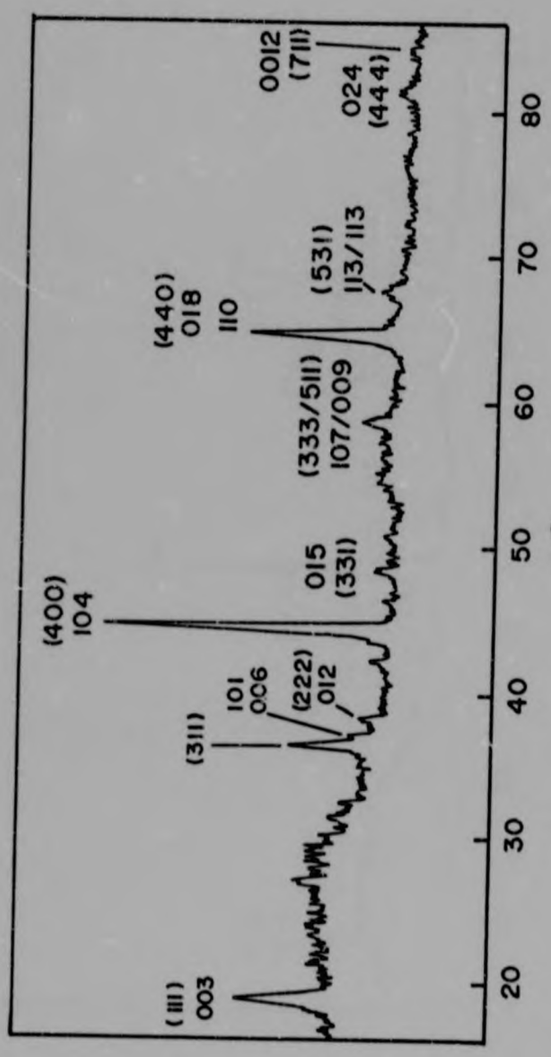

FIG. 7.3
X-ray diffraction pattern of $Li_{0.45}V_2O_4$

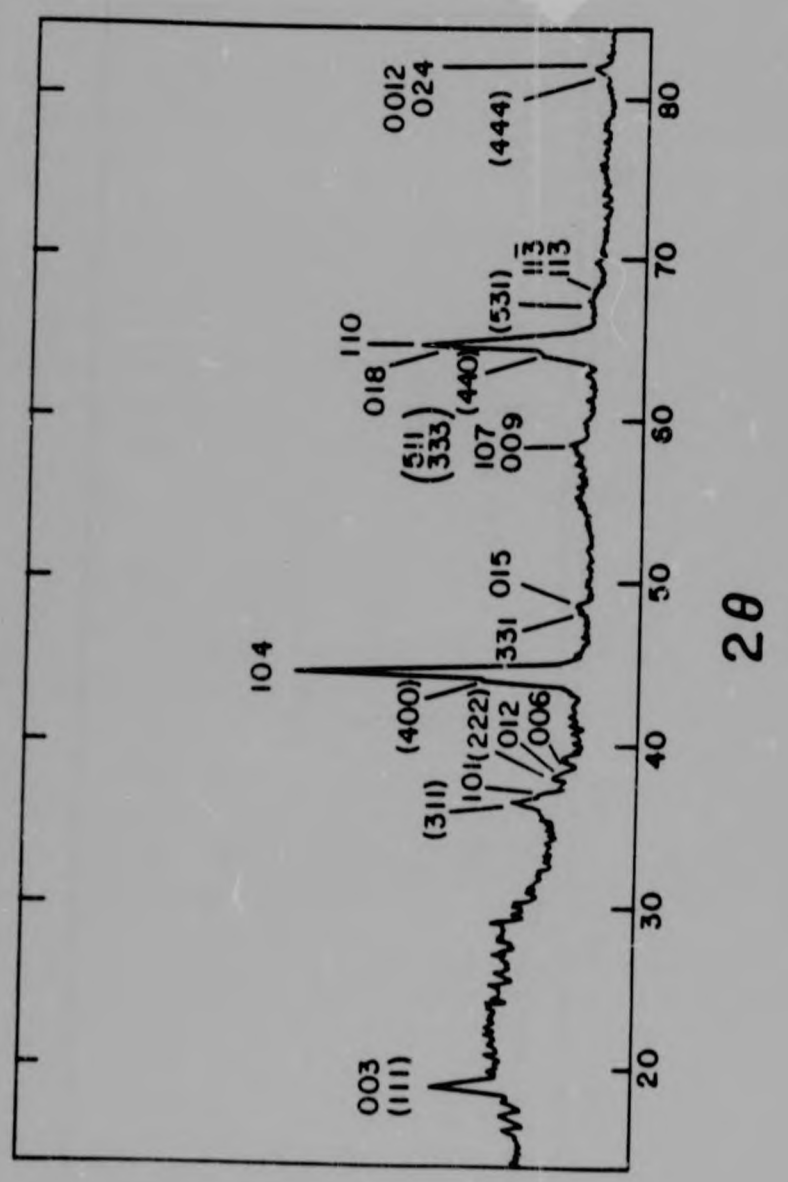

FIG. 7.4
X-ray diffraction pattern of $Li_{0.27}V_2O_4$ (two-phase)

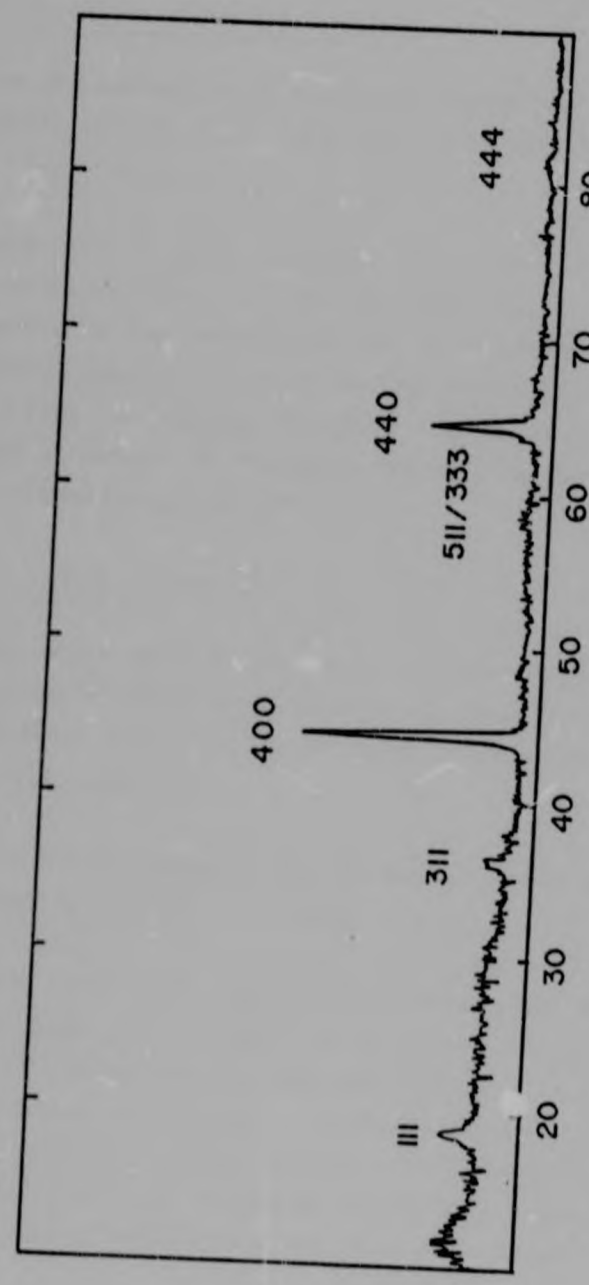

FIG. 7.5
X-ray diffraction pattern of $Li_{0.28}V_2O_4$ (cubic)

7.4 INTERPRETATION OF THE STRUCTURAL DATA

7.4.1 $Li_{1-x}V_2O_4$, where $0 < x < 0.34$

Lithium extraction up to a typical composition $Li_{0.66}V_2O_4$ leads to a cubic pattern (Fig. 7.2), similar to that of the parent compound $Li_{\sim 1.0}V_2O_4$.

The retention of cubic symmetry, the linear contraction of the cell constants (Fig. 7.1) and the essentially unchanged relative intensities of the reflections are all evidence for retention of the spinel $[B_2]X_4$ framework during delithiation. Lithium is removed from the $Li[V_2]O_4$ structure via the interconnected three-dimensional network of 8a-16c-8a channels as previously observed in the system $Li_{1-x}Mn_2O_4$ [74-76].

7.4.2 $Li_{1-x}V_2O_4$, where $0.34 < x < 0.77$

The cubic phase observed in samples derived from $Li_{\sim 1.0}V_2O_4$ will be discussed in detail in Section 7.4.3. Only the two-phase material obtained from lithium-deficient spinels (e.g. $Li_{0.95}V_2O_4$) will be discussed here.

The cubic phase indexes to the spinel Fd3m space group, the trigonal phase to the $R\bar{3}m$ space group.

As lithium extraction progresses, the proportion of the trigonal phase increases and a drastic change in the relative intensities of several reflections is observed (Fig. 7.4). In particular, the intensities of the cubic/trigonal {111}/{003} and {311}/{101} reflections decrease significantly; the intensity of the {400}/{104} reflection also decreases, though to a lesser extent, when compared to the {440}/({110} and {018} reflections.

Because of the severe overlap of the cubic and trigonal phases, a precise structural determination could not be undertaken on these samples. However, a number of observations can be made.

Firstly, the cell constants of the trigonal phase are very similar to those of $Li_{0.2}VO_2$ (cf Chapter 4). The relative intensities of LiV_2O_4, $Li_{0.27}V_2O_4$ and $Li_{0.2}VO_2$ were normalised to 1000 for the {440} reflection of the cubic phase (or the {018/110} reflection of the trigonal phase) (Table 8.2). As all the atoms in that plane scatter in phase (cf Appendix), it is possible to compare the relative intensities of the reflections in the three compounds.

TABLE 7.2

Relative intensities of LiV_2O_4, $Li_{0.27}V_2O_4$, and $Li_{0.2}VO_2$

{hkl} cubic	LiV_2O_4	$Li_{0.27}V_2O_4$	$Li_{0.2}VO_2$	{hkl} trigonal
111	1978	654	241	003
311	1205	379	145	101
222	175	86	69	006 ; 012
400	1708	1324	1902	104
331	181	98	32	015
551	370	133	47	009 ; 107
440	1000	1000	1000	018 ; 110
531	283	111	57	113 ; $11\bar{3}$
444	221	123	160	0 0 12 ; 024

It is immediately evident that the intensity distribution in $Li_{0.27}V_2O_4$ has altered significantly from that of the parent compound LiV_2O_4. In particular, the intensities of the cubic {111}, {311} and {222} reflections are considerably nearer to the corresponding trigonal reflections in $Li_{0.2}VO_2$ than to the spinel parent compound LiV_2O_4.

It is to be noted that the stoichiometry $Li_{0.27}V_2O_4$ can also be expressed as $Li_{0.14}VO_2$, which is relatively close to the delithiated phase $Li_{0.2}VO_2$, obtained from the layered compound $LiVO_2$.

On the basis of the evidence presented above, it is suggested that, for $x>0.33$ in $Li_{1-x}V_2O_4$, approximately one-ninth of the vanadium cations in the 16d sites of the vanadium-rich layer migrates to the 16c sites of an adjacent layer, thereby changing the distribution of vanadium cations in alternate layers from the 3:1 spinel ratio to a 2:1 ratio, as in $Li_{0.22}VO_2$.

7.4.3 Structure of $Li_{0.28}V_2O_4$

Single-phase samples with low lithium content ($0.72<x<0.77$ in $Li_{1-x}V_2O_4$) were obtained from spinels with the composition $Li_{1.0}V_2O_4$. The unit cell was cubic, with a typical cell constant of a = 8.151(3) Å (Table 7.1). This represents a volume contraction of 3% in the course of delithiation. A typical X-ray pattern of this material is shown in Fig. 7.5. The relative intensities of the peaks differed sharply from those of LiV_2O_4, and followed the general trend already observed in the two-phase samples of similar composition.

The sample $Li_{0.28}V_2O_4$ was selected for a structure refinement, although only a few reflections are clearly defined. The paucity of the data (9 intensities, corresponding to 10 reflections) limited the amount of information which could be extracted from the refinement. However, good indications on the location of the vanadium cations were obtained.

In the course of a preliminary cycle, the oxygen positional parameter and the B_{iso} factor were refined, obtaining the values u = 0.254(4) and B_{iso} = 2.6(2.0). In subsequent cycles, these parameters were fixed at u = 0.254 and B_{iso} = 3.0. The temperature factors of lithium and vanadium were maintained at

1.0 and 0.5 respectively, whilst 0.28 Li^+ ions were placed in the tetrahedral 8a sites.

The $V^{3+/4+}$ cation occupancy was initially allowed to vary in the 16c and 16d octahedral sites; the total number of vanadium cations was fixed at 2.0. A vanadium-ion distribution of 1.56(9) in the 16d sites and 0.44(9) in the 16c sites was obtained. In view of the rather high R factor for this model (viz. 21.4%), another refinement was carried out, where the vanadium cations were allowed to occupy the tetrahedral 8a positions as well as the octahedral 16c and 16d sites. The sum of the vanadium ion occupancies was unconstrained. This refinement led to a greatly improved R factor of 14.4%. The full structural parameters are listed in Table 7.3a, calculated and observed intensities in Table 7.3b.

In this model 0.13(5) vanadium cations are located in the tetrahedral 8a sites, 0.42(7) are in the 16c octahedra and 1.49(13) are in the 16d sites. It is interesting to note that the sum of the vanadium cations, viz. 2.04(25), is in excellent agreement with the stoichiometry $Li_{0.28}V_2O_4$.

Better fits could not be obtained, due to the poor quality of the data.

TABLE 7.3a

Structural parameters of $Li_{0.28}V_2O_4$

R = 14.4%

Space-group: Fd3m (O_h^7) a = 8.151(3) Å

Atom	Position	x	y	z	B(Å^2)	n
Li^+	8a	0.125	0.125	0.125	1.0	0.28
V^{5+}	8a	0.125	0.125	0.125	0.5	0.13(5)
$V^{3+/4+}$	16c	0.000	0.000	0.000	0.5	0.42(7)
$V^{3+/4+}$	16d	0.500	0.500	0.500	0.5	1.49(13)
O^{2-}	32e	0.254(4)	0.254(4)	0.254(4)	2.6(2.0)	4.0

TABLE 7.3b

X-ray diffraction pattern of $Li_{0.28}V_2O_4$ with calculated and observed intensities

hkl	d_{obs}*	d_{calc}	I_{obs}	I_{calc}
111	4.712	4.706	487	454
311	2.462	2.578	348	416
222	-	2.353	57	54
400	2.038	2.038	1312	1381
331	-	1.870	59	49
511 } 333	-	1.569	176	144
440	1.440	1.441	993	749
444	-	1.176	132	152
840	-	0.911	158	213

* Not indicated in the case of weak and diffuse peaks.

7.5 ELECTROCHEMICAL CHARACTERISATION

7.5.1 Electrochemical Curve

The electrochemical curve, where the open-circuit voltage (o.c.v.) is plotted against the composition, x, in $Li_{1-x}V_2O_4$, is shown in Fig. 7.6. It is to be noted that the starting material was slightly lithium-deficient.

The electrochemical curve comprises three distinct stages. Region I, which extends between $0 < x \leq 0.3$, represents a single phase reaction product, in agreement with the structural data. In this section, lithium is extracted from $Li[V_2]O_4$ whilst the $[V_2]O_4$ framework is maintained.

Region II ($0.3<x<0.75$) appears to be a two-phase region: structural evidence (sections 7.3 and 7.4) shows the presence of two phases in samples derived from a lithium-deficient spinel. The

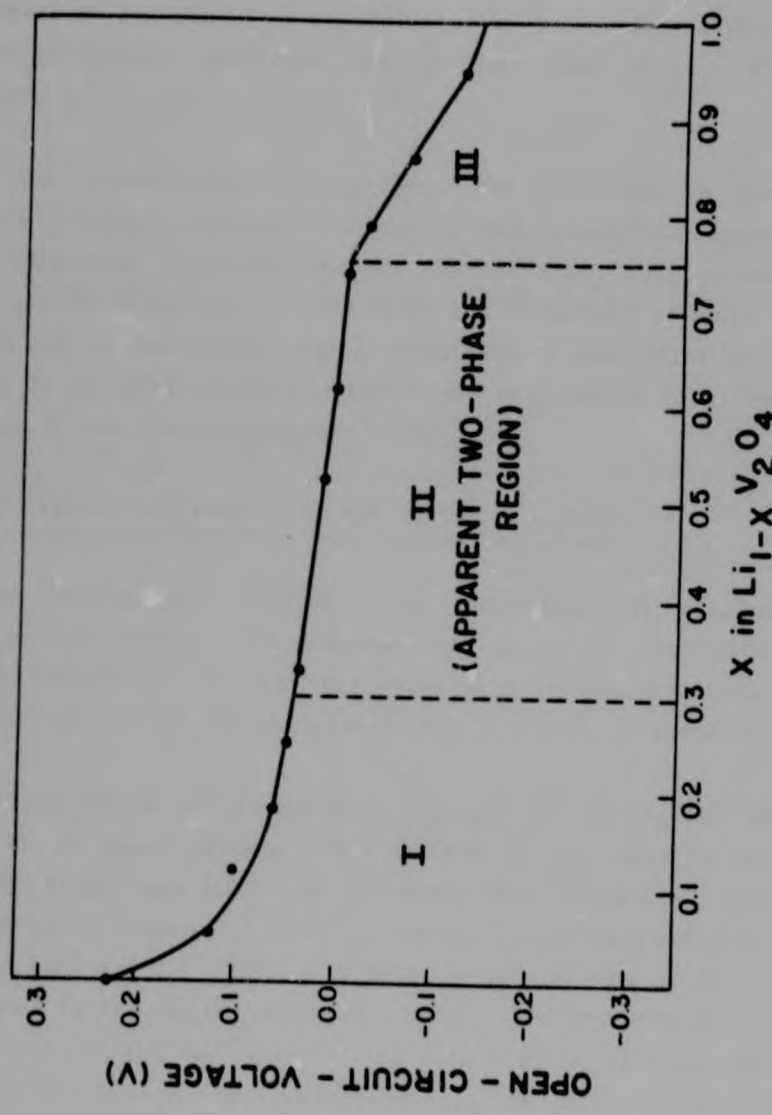

FIG. 7.6

Ambient temperature electrochemical curve of the cell $Li_{\sim 0.95}V_2O_4$ / $LiClO_4$ 1M (P.C.) / $LiMn_2O_4$

trigonal phase results from the migration of vanadium cations from one layer to the next: this process leads to a reduction of the crystal symmetry from cubic to trigonal. The simultaneous presence of two phases is probably due to the preferred delithiation of smaller particles, as in the cases of $Li_{1-x}VO_2$ (cf Section 4.5.1) and $Li_{1-x}Mn_2O_4$ [75].

For the composition $Li_{\sim 0.25}V_2O_4$, the structure is predominantly trigonal. Delithiation beyond this composition appears as a single-phase electrode process (Region III), that extends to the stoichiometry V_2O_4. Although the structure of this phase could not be determined, due to insufficient quantities of material, it is likely to be similar to VO_2 prepared by total delithiation of the layered compound $LiVO_2$ [133].

7.5.2 Cyclic Voltammetry of the System $Li_{1\pm x}V_2O_4$

Cyclic voltammetry studies were undertaken on samples of $Li_{\sim 1.0}V_2O_4$. Cyclic voltammograms of $Li_{1+x}V_2O_4$ were discussed in section 6.5.3. In this chapter, lithium extraction from LiV_2O_4, as well as the combined system $Li_{1\pm x}V_2O_4$ is presented.

The first series of experiments consists of an initial anodic scan to an upper voltage limit of 4.00 V, followed by cycling between 4.00 V and 1.20 V at different scan rates (viz. 0.5 and 1.0 mV/sec). Figure 7.7 shows a typical cyclic voltammogram with a scan rate v = 0.5 mV/sec. A broad oxidation peak at 3.67 V is assigned to the delithiation of LiV_2O_4. The shoulder at 3.49 V might reflect the beginning of the migration of vanadium cations through the layers. Upon scan reversal, the delithiation process is shown to be irreversible. However, a very diffuse, shallow reduction peak is observed at ~2.0 V.

The irreversibility of the delithiation process is due to the loss of the $[V_2]O_4$ spinel sublattice, which is caused by the

migration of $V^{3+/4+}$ to adjacent layers. The reduction peak observed at ~2.0 V is due to the relithiation of the modified structure. This lithiation process is shown to be reversible, with a corresponding oxidation peak at ~2.3 V.

A similar voltammogram was obtained with a scan rate of 1 mV/sec (Fig. 7.8); in this case, the peaks due to relithiation of the delithiated structure and the related re-oxidation were slightly more intense, but situated further apart (with maxima at ~1.8 and ~2.9 V respectively). The shape of these peaks and the large potential difference between them indicate that this reaction is limited by a slow lithium diffusion rate.

Cyclic voltammograms at the scan rates 1 mV/sec, 0.5 mV/sec and 0.1 mV/sec of the complete system $Li_{1\pm x}V_2O_4$ ($0<x<1$) are shown in Figs 7.9 - 7.11. The initial scan was cathodic, with upper and lower switching potentials of 1.20 V and 4.00 V respectively.

The lithiation and delithiation peaks of the first and subsequent cycles, described above, are clearly visible in Fig. 7.9 (v = 1 mV/sec). One differing feature of the voltammogram is the peak corresponding to lithium extraction from LiV_2O_4. The current maximum at 3.58 V is followed by a distinct shoulder at a higher potential (3.74 V). This contrasts the voltammograms with an initial anodic scan described above (Figs 7.7 - 7.8), where a shoulder occurs at a lower potential than the main peak.

Figure 7.10 shows a cyclic voltammogram of $Li_{1\pm x}V_2O_4$ recorded at a scan rate of 0.5 mV/sec. A striking feature is the splitting of the second oxidation process into a doublet, which does not appear when cycling is initiated with an anodic scan (Fig. 7.7). The two current maxima at 3.59 V and 3.69 V are of approximately the same intensity.

This observation indicates that the first lithiation and subsequent delithiation of LiV_2O_4 provokes a structural modification

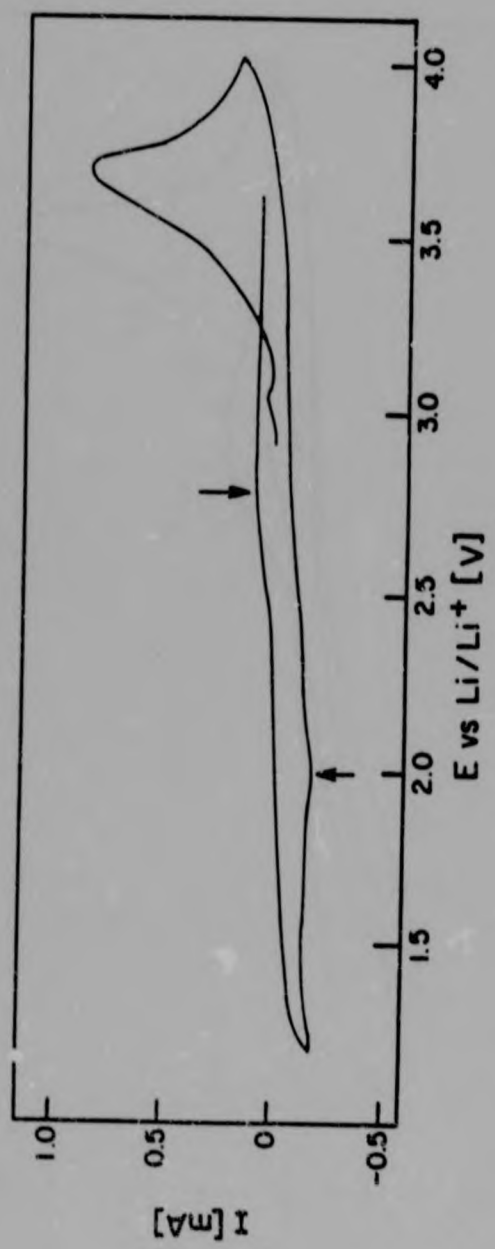

FIG. 7.7
Cyclic voltammogram of the system $Li_{1\pm x}V_2O_4$ (initial scan anodic; v = 0.5 mV/sec)

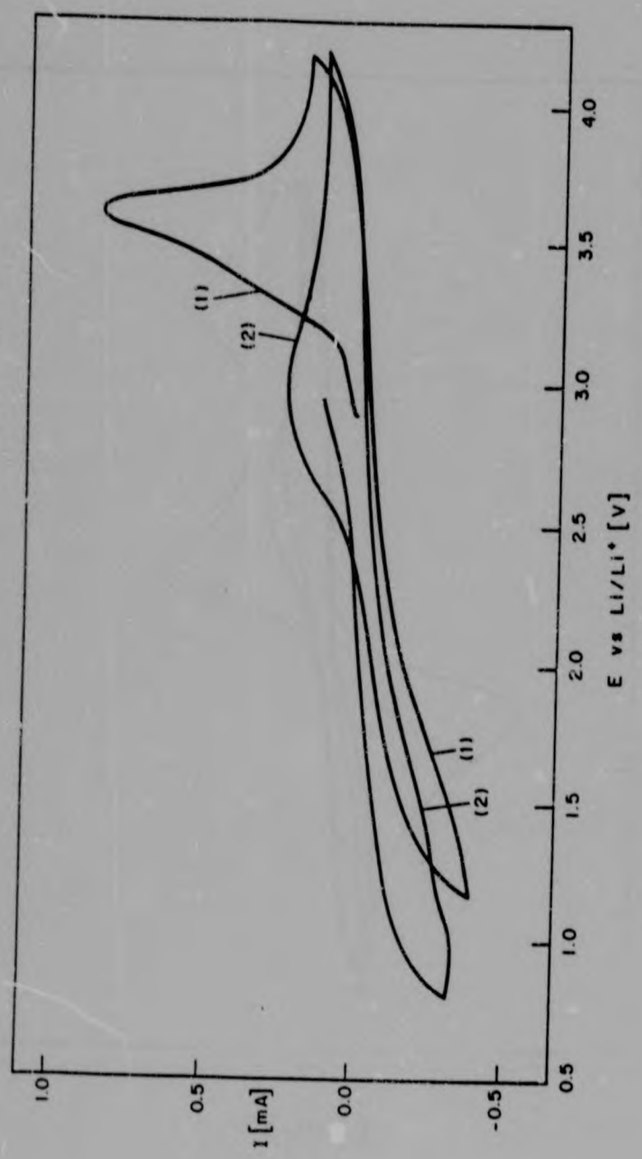

FIG. 7.8
Cyclic voltammogram of the system $Li_{1\pm x}V_2O_4$ (initial scan anodic; v = 1.0 mV/sec)

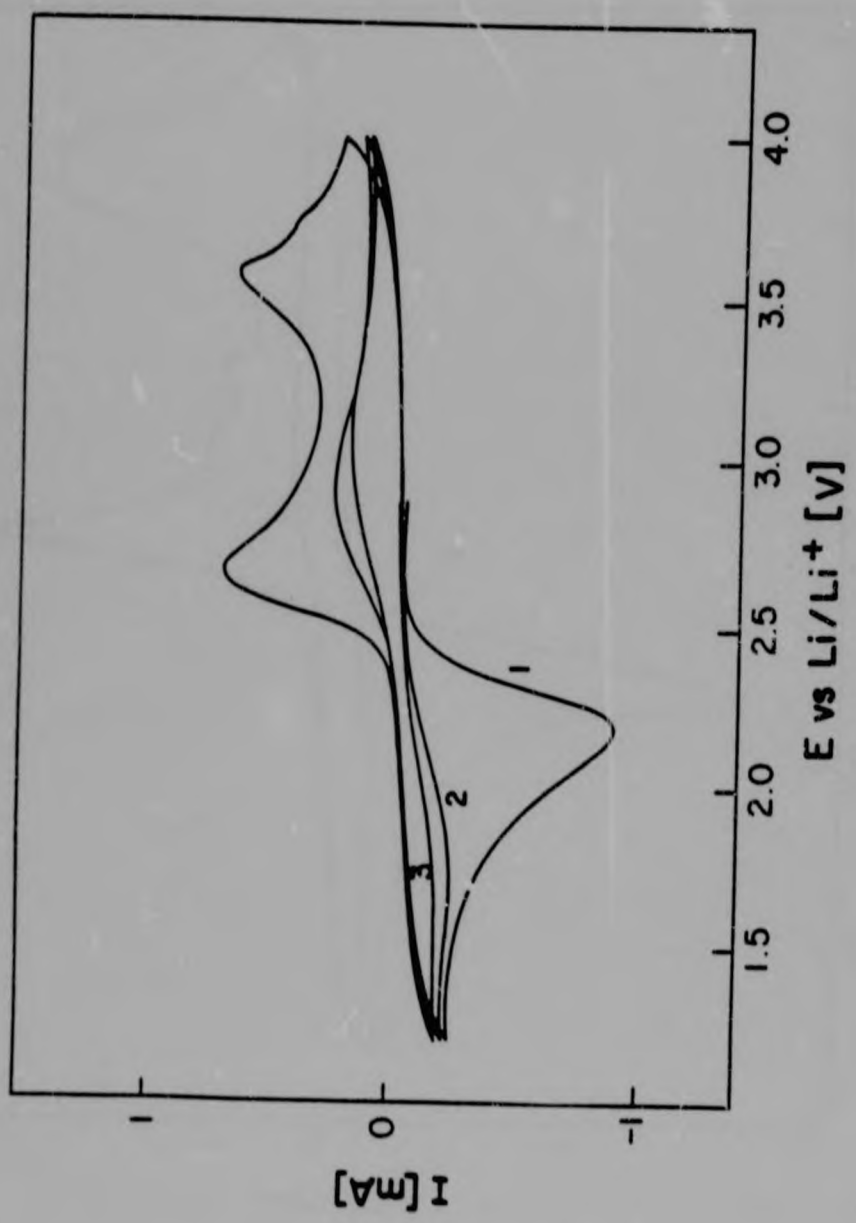

FIG. 7.9
Cyclic voltammogram of the system $Li_{1\pm x}V_2O_4$ (initial scan cathodic; v = 1.0 mV/sec)

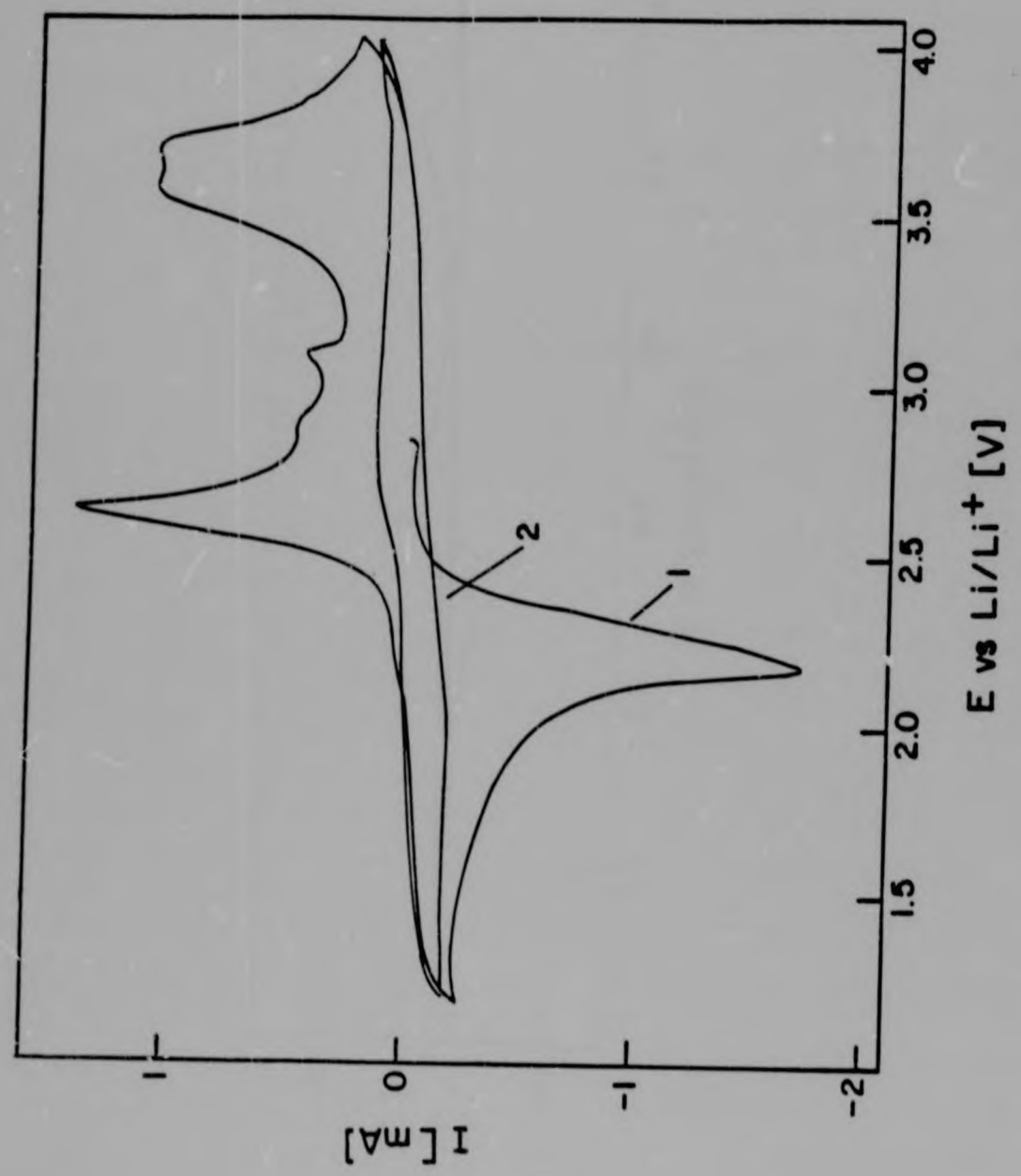

FIG. 7.10
Cyclic voltammogram of the system $Li_{1\pm x}V_2O_4$ (initial scan cathodic; v = 0.5 mV/sec)

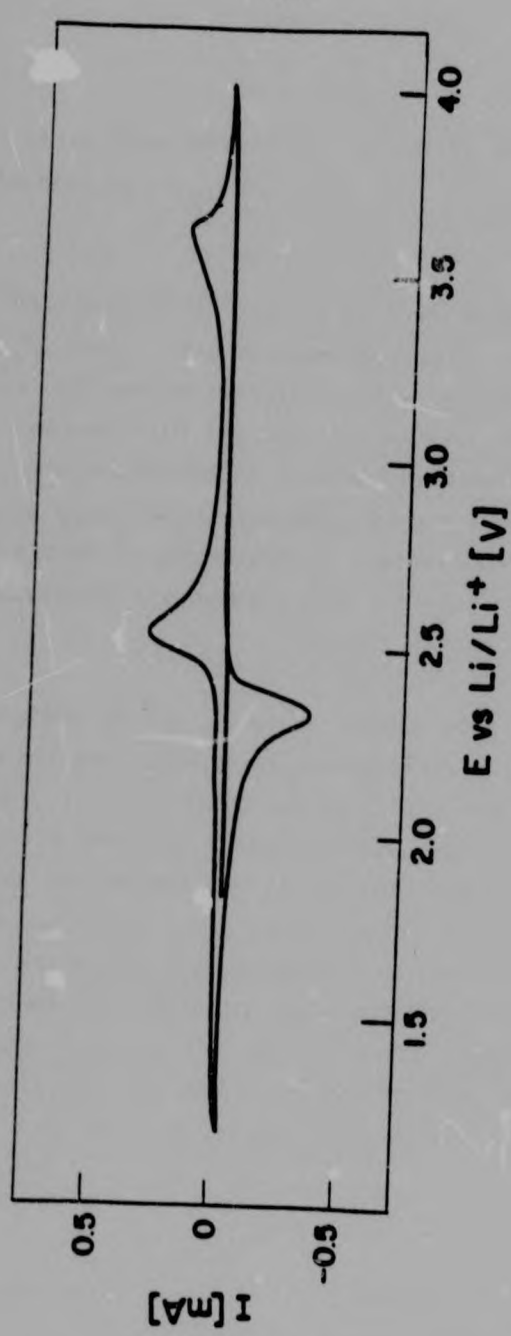

FIG. 7.11

Cyclic voltammogram of the system $Li_{1\pm x}V_2O_4$ (initial scan cathodic; v = 0.1 mV/sec)

in the spinel, which then affects the mechanism of the delithiation process leading to $Li_{1-x}V_2O_4$.

In an attempt to identify the nature of this structural change, samples of LiV_2O_4 were cycled chemically, using n-BuLi and Br_2. The powder X-ray diffraction patterns of the cycled products thus obtained were compared with the parent compound LiV_2O_4 and with samples of the same stoichiometry obtained by direct delithiation of LiV_2O_4. These experiments, however, did not reveal any significant changes either in the symmetry, the cell constants or the relative intensities of the peaks.

Cyclic voltammograms of $Li_{1\pm x}V_2O_4$ at slower scan rates (v = 0.1 mV/sec) are not particularly revealing (Fig. 7.11). Only the first three peaks, i.e. the reduction at 2.32 V and two oxidation processes at 2.53 V and 3.63 V respectively, were observed. The second cycle does not exhibit any peaks: the reversible reduction process observed at higher scan rates was not visible. This is not surprising, since the peak intensity is proportional to the square root of both the diffusion rate and the sweep rate. For the same electrode area, in the case of a diffusion-limited process, the intensity of the peaks should therefore decrease with the ratio 3:2:1 when the scan rates v =1.0 mV/sec, 0.5 mV/sec and 0.1 mV/sec are used.

The two additional small peaks at ~3 V which are most clearly visible in Fig. 7.9 are attributed to a minor impurity phase, as these peaks were not always present in the voltammograms of other LiV_2O_4 samples.

in the spinel, which then affects the mechanism of the delithiation process leading to $Li_{1-x}V_2O_4$.

In an attempt to identify the nature of this structural change, samples of LiV_2O_4 were cycled chemically, using n-BuLi and Br_2. The powder X-ray diffraction patterns of the cycled products thus obtained were compared with the parent compound LiV_2O_4 and with samples of the same stoichiometry obtained by direct delithiation of LiV_2O_4. These experiments, however, did not reveal any significant changes either in the symmetry, the cell constants or the relative intensities of the peaks.

Cyclic voltammograms of $Li_{1\pm x}V_2O_4$ at slower scan rates (v = 0.1 mV/sec) are not particularly revealing (Fig. 7.11). Only the first three peaks, i.e. the reduction at 2.32 V and two oxidation processes at 2.53 V and 3.63 V respectively, were observed. The second cycle does not exhibit any peaks: the reversible reduction process observed at higher scan rates was not visible. This is not surprising, since the peak intensity is proportional to the square root of both the diffusion rate and the sweep rate. For the same electrode area, in the case of a diffusion-limited process, the intensity of the peaks should therefore decrease with the ratio 3:2:1 when the scan rates v =1.0 mV/sec, 0.5 mV/sec and 0.1 mV/sec are used.

The two additional small peaks at ~3 V which are most clearly visible in Fig. 7.9 are attributed to a minor impurity phase, as these peaks were not always present in the voltammograms of other LiV_2O_4 samples.

7.5.3 Lithium Diffusion Rate in $Li_{0.28}V_2O_4$

The lithium-ion diffusion rate in $Li_{0.28}V_2O_4$ amounts to 1.10^{-9} cm^2/sec. It is considerably faster than in the spinel $Li[V_2]O_4$, where $\tilde{D} = 4.10^{-10}$ cm^2/sec, but slower than in the disordered rocksalt phase $Li_2[V_2]O_4$, where $\tilde{D} = 6.10^{-8}$ cm^2/sec (cf section 6.5.4). The latter finding is perhaps a little surprising, as the defect rocksalt structure might have been anticipated to be a faster Li^+ conductor, since it contains more vacant sites. The lithium-deficient $Li_{0.28}V_2O_4$ compound is also slower than the layered compound $LiVO_2$ ($\tilde{D} = 5.10^9$ cm^2/sec), where the intersite potential barriers are probably lower than in a rocksalt phase.

7.6 DISCUSSION

Lithium extraction from LiV_2O_4 can be achieved chemically and electrochemically. Samples of $Li_{1-x}V_2O_4$ ($0<x\leq0.73$) have been characterised by powder X-ray diffraction; the reaction mechanism and its products have been studied by electrochemical methods.

Lithium extraction proceeds in two steps. In the region $Li_{1-x}V_2O_4$ ($0<x<0.33$), lithium is extracted from the A-sites of the spinel, without altering the $[B_2]X_4$ framework. As delithiation continues beyond $x \approx 0.33$ in $Li_{1-x}V_2O_4$, a fraction of the vanadium cations migrates from the 16d sites of a vanadium-rich layer to the 16c sites of the adjacent layer: the vanadium distribution in alternate layers changes from a 3:1 to a 5:3 ratio. Chemical lithium extraction from the spinel LiV_2O_4 thus leads to the compound $Li_{0.28}V_2O_4$, which is similar both in structure and in composition to the phase $Li_{0.2}VO_2$, obtained by delithiation of the layered material $LiVO_2$. The transfer of vanadium cations is necessary to stabilise the delithiated structure: this phenomenon has already been observed in the course of this work in the case of the system $Li_{1-x}VO_2$ (cf chapter 4).

7.5.3 Lithium Diffusion Rate in $Li_{0.28}V_2O_4$

The lithium-ion diffusion rate in $Li_{0.28}V_2O_4$ amounts to 1.10^{-9} cm^2/sec. It is considerably faster than in the spinel $Li[V_2]O_4$, where $\tilde{D} = 4.10^{-10}$ cm^2/sec, but slower than in the disordered rocksalt phase $Li_2[V_2]O_4$, where $\tilde{D} = 6.10^{-8}$ cm^2/sec (cf section 6.5.4). The latter finding is perhaps a little surprising, as the defect rocksalt structure might have been anticipated to be a faster Li^+ conductor, since it contains more vacant sites. The lithium-deficient $Li_{0.28}V_2O_4$ compound is also slower than the layered compound $LiVO_2$ ($\tilde{D} = 5.10^9$ cm^2/sec), where the intersite potential barriers are probably lower than in a rocksalt phase.

7.6 DISCUSSION

Lithium extraction from LiV_2O_4 can be achieved chemically and electrochemically. Samples of $Li_{1-x}V_2O_4$ ($0<x<0.73$) have been characterised by powder X-ray diffraction; the reaction mechanism and its products have been studied by electrochemical methods.

Lithium extraction proceeds in two steps. In the region $Li_{1-x}V_2O_4$ ($0<x<0.33$), lithium is extracted from the A-sites of the spinel, without altering the $[B_2]X_4$ framework. As delithiation continues beyond $x \approx 0.33$ in $Li_{1-x}V_2O_4$, a fraction of the vanadium cations migrates from the 16d sites of a vanadium-rich layer to the 16c sites of the adjacent layer: the vanadium distribution in alternate layers changes from a 3:1 to a 5:3 ratio. Chemical lithium extraction from the spinel LiV_2O_4 thus leads to the compound $Li_{0.28}V_2O_4$, which is similar both in structure and in composition to the phase $Li_{0.2}VO_2$, obtained by delithiation of the layered material $LiVO_2$. The transfer of vanadium cations is necessary to stabilise the delithiated structure: this phenomenon has already been observed in the course of this work in the case of the system $Li_{1-x}VO_2$ (cf chapter 4).

If migration of the vanadium cations through the octahedral edges is excluded, then it must take place in a 48f tetrahedral site. As previously discussed in detail (section 4.4.2), V^{4+} cations are not stable in a tetrahedral environment, but probably disproportionate according to the energetically accessible reaction [137]:

$$2\ V^{4+} \longrightarrow V^{5+} + V^{3+}$$

In the case of $Li_{1-x}VO_2$, some of the tetrahedra share faces with three empty octahedral sites: this facilitates the transfer of the vanadium cations through the former. By contrast, in the spinel structure, the 48f tetrahedra share faces with two occupied 16d and two vacant 16c octahedra: this initially makes the migration from the 16d sites via the 48f tetrahedra more difficult than in $Li_{1-x}VO_2$, due to the repulsion between V^{5+} and $V^{3+/4+}$ cations situated in face-sharing tetrahedral and octahedral sites respectively. The predicted relative ease of lithium extraction is confirmed by cyclic voltammetry results, where it is shown that delithiation occurs at lower potentials in $LiVO_2$ than in the case of LiV_2O_4 (oxidation potentials: 3.09 V for $LiVO_2$ and 3.67 V for LiV_2O_4, v = 1 mV/sec).

It would be reasonable to assume that vanadium-ion migration would occur more readily in the case of the lithium-deficient spinels $Li_{1-x}V_2O_4$ ($0<x<0.10$), which have the structure $(Li_{1-x}V_x)_{8a}\ [V_{2-x}\ \square_x]O_4$, than in the case of $Li[V_2]O_4$. In the former, a few 48f tetrahedra share faces with only one occupied octahedral 16d site, from which the vanadium cation can migrate with greater ease. Although the results presented here do not constitute conclusive evidence, they support this hypothesis to a certain extent. The structural data given in Table 7.1 shows that the trigonal phase is present in an appreciable quantity in a compound $Li_{0.45}V_2O_4$, derived from the lithium-

deficient $Li_{0.95}V_2O_4$: it is not clearly visible in material of the same composition (viz. $Li_{0.46}V_2O_4$), prepared from $Li_{\sim 1.0}V_2O_4$.

7.7 CONCLUSIONS

In this chapter, it is shown that, as in the case of $LiTi_2O_4$ and $LiMn_2O_4$, it is possible to extract lithium from LiV_2O_4. In this section, a brief comparison between the three oxo-spinels is drawn.

Delithiation of LiV_2O_4 occurs in two stages. Initially, the spinel $[B_2]X_4$ framework is maintained, up to the composition $Li_{0.67}[V_2]O_4$. Further delithiation is accompanied by the migration of a fraction of vanadium cations through the layers. This results in the formation of a trigonal phase, similar to $Li_{1-x}VO_2$ (cf chapter 4).

A similar rearrangement probably occurs in $Li_{1-x}Ti_2O_4$: the delithiated compound $Li_{0.1}Ti_2O_4$ is reported to be poorly crystalline and probably has a similar structure to $Li_{1-x}VO_2$ [77, 78]. This suggests that a migration of titanium cations through the layers takes place in the course of the delithiation. No electrochemical work on the system $Li_{1-x}Ti_2O_4$ has been reported to date in the literature.

In the case of the third isostructural lithium spinel, $Li[Mn_2]O_4$, the situation is quite different; all the lithium can be removed from $Li[Mn_2]O_4$ without altering the spinel $[B_2]X_4$ framework. A new polymorph of manganese dioxide, λ-MnO_2, is formed, which has the spinel sub-lattice structure $[Mn_2]O_4$ [74-76, 163]. In λ-MnO_2 the 8a-16c-8a channels remain available for lithium diffusion, allowing reversible lithiation to form $Li[Mn_2]O_4$ and, subsequently, $Li_2[Mn_2]O_4$. The reaction has been shown to be reversible by cyclic voltammetry (Fig. 6.11), where delithiation of $Li[Mn_2]O_4$ occurred at E = 4.1 V with a corresponding re-lithiation at E = 3.8 V [100]:

$$2\lambda\text{-}MnO_2\ (=[Mn_2]O_4) \underset{}{\overset{2Li}{\rightleftharpoons}} Li_2[Mn_2]O_4$$

A system of this type is obviously very attractive as an electrode in a secondary lithium cell. In the case of LiV_2O_4, the partial loss of the $[B_2]X_4$ framework for the compositions $Li_{1-x}V_2O_4$ (where $x > 0.33$) limits the reversibility of the $Li_{1\pm x}V_2O_4$ system. Cyclic voltammetry experiments clearly show that, whilst lithiation of LiV_2O_4 is reversible, delithiation is an irreversible process. Subsequent lithiation of $Li_{1-x}V_2O_4$ ($x \approx 0.25$) occurs by a different mechanism and appears to be reversible. A study of this reaction is reported elsewhere [174].

Although the reversible range of the system $Li_{1\pm x}V_2O_4$ is smaller than in the system $Li_{1\pm x}Mn_2O_4$, the galvanostatic discharge curve of LiV_2O_4 (section 6.5.2) shows a considerably better operating voltage than that observed for $LiMn_2O_4$, i.e. 2.4 V as opposed to 0.3 V [81]. It would therefore be of practical interest to extend the stability range of the $[B_2]X_4$ framework in the vanadium compound. Attempts to achieve this result are described in the following chapter.

$$2\lambda\text{-}MnO_2\ (=[Mn_2]O_4) \underset{}{\overset{2Li}{\rightleftharpoons}} Li_2[Mn_2]O_4$$

A system of this type is obviously very attractive as an electrode in a secondary lithium cell. In the case of LiV_2O_4, the partial loss of the $[B_2]X_4$ framework for the compositions $Li_{1-x}V_2O_4$ (where $x > 0.33$) limits the reversibility of the $Li_{1\pm x}V_2O_4$ system. Cyclic voltammetry experiments clearly show that, whilst lithiation of LiV_2O_4 is reversible, delithiation is an irreversible process. Subsequent lithiation of $Li_{1-x}V_2O_4$ ($x \approx 0.25$) occurs by a different mechanism and appears to be reversible. A study of this reaction is reported elsewhere [174].

Although the reversible range of the system $Li_{1\pm x}V_2O_4$ is smaller than in the system $Li_{1\pm x}Mn_2O_4$, the galvanostatic discharge curve of LiV_2O_4 (section 6.5.2) shows a considerably better operating voltage than that observed for $LiMn_2O_4$, i.e. 2.4 V as opposed to 4.3 V [81]. It would therefore be of practical interest to extend the stability range of the $[B_2]X_4$ framework in the vanadium compound. Attempts to achieve this result are described in the following chapter.

CHAPTER 8

FORMATION AND DELITHIATION OF $Li_xZn_yV_2O_4$ ($0.73 < x < 0.84$; $0.04 < y < 0.10$)

8.1 INTRODUCTION

8.1.1 Choice of Zinc as a Dopant

The aim of this work, proposed in section 7.7, is to stabilise the $[B_2]X_4$ framework of delithiated $Li_{1-x}V_2O_4$, with $x>0.34$. In order to achieve this goal, it is necessary to prevent the migration of vanadium cations through the layers.

It has been observed in both $Li_{1-x}VO_2$ and $Li_{1-x}V_2O_4$ (cf chapters 4 and 7) that the vanadium cations transfer to the adjacent layer when the latter becomes cation-deficient. At this point, the electrostatic cation-anion interactions of the remaining cations are no longer sufficient to bond the layers of oxide anions, and it becomes necessary to replace the extracted lithium cations with a few vanadium ions.

The introduction of a small, di- or even trivalent cation, with a strong preference for tetrahedral sites, is anticipated to provide sufficient electrostatic bonding between oxide layers in the delithiated structure. This would render unnecessary the transfer of vanadium ions from the B sites to the cation-deficient layer of $Li_{1-x}V_2O_4$ ($x>0.34$).

Zinc was selected as an appropriate dopant for the following reasons:

a) Zn^{2+} has a strong preference for tetrahedral sites in oxides, and is therefore anticipated to occupy the A sites of the spinel.

b) The ionic radius of Zn^{2+} (0.60 Å) is practically identical to that of Li^{+} (0.59 Å); the introduction of Zn^{2+} in the place of Li^{+} should therefore not perturb the structure.

c) Zn^{2+} is a divalent cation: the electrostatic interactions between Zn^{2+} and the oxide anions will therefore be relatively strong.

In addition, Zn^{2+} is anticipated to be less mobile than Li^{+}, firstly because of its strong preference for tetrahedral coordination, and secondly because it is divalent and therefore more strongly bonded. It should therefore be reluctant to move from the A sites, in the course of the delithiation.

8.1.2 Literature Survey of Solid Solutions with LiV_2O_4

A number of solid solutions containing LiV_2O_4 as an end-member are reported in the literature: their structural characteristics and methods of preparation will be briefly recalled here.

Reuter and Jaskowsky were the first to investigate solid solutions of vanadium spinels: the formation of the solid solution $Li_xMg_{1-x}[V_2]O_4$ ($0<x<1$) was reported in 1960 [147]. A comprehensive study of the systems $M[M'_xV^{4+}_xV^{3+}_{2-2x}]O_4$, where M, M' = Mg, Zn, Co, Mn, Cd, Ni and Fe and including the system $Li_xMg_{1-x}[V_2]O_4$ was published in 1965 [175]. These spinels were generally prepared by heating a mixture of the metal oxides under vacuum to temperatures of 800 °C - 1 200 °C [175]. The crystal structure and the electrical properties of these solid solutions were described. A further study of the electronic conductivity of $Li_xMg_{1-x}[V^{3+}_{2-x}V^{4+}_x]O_4$ gives a more detailed description of the preparation of these compounds: the end-members LiV_2O_4 and MgV_2O_4 were heated together between 600 °C and 900 °C under vacuum.

The electrical properties of the lithium-cobalt vanadium spinel $Co_{1-x}Li_xV_2O_4$ ($0<x<1$) were investigated by Rogers et al. [176]

Compounds of this type were prepared by heating the oxides at 650 °C - 750 °C under vacuum. In a study of the solid state reactions of cadmium oxides with VO, V_2O_3 and VO_2, Reuter and Müller report an attempt to prepare a solid solution by heating the spinels CdV_2O_4 and LiV_2O_4 to 700 °C in an evacuated silica tube. Only a limited solubility (ca. 5 mol%) was observed at either end of the phase diagram [177]. In contrast, the solid solutions $Li_xFe_{1-x}V_2O_4$ and $Li_xMn_{1-x}V_2O_4$ extended over the full range ($0<x<1$). Both series can be prepared by heating the spinel end-members at high temperatures (700 °C - 750 °C) [149, 178].

Over the years, a few papers on lithium-zinc vanadium oxides have appeared. Physical properties of the system $Li_xZn_{1-x}[V^{3+}_{2-x}V^{4+}_x]O_4$ ($0<x<1$) were first described by Reuter and Müller [179]. In that paper, however, the method of preparation is not given.

In a later report, Pollert [150] described the preparation and properties of $LiM_xV_{2-x}O_4$ ($0<x<0.5$) where M = Zn and Mg. These compounds were synthesised by heating mixtures of ZnO or MgO with stoichiometric quantities of $LiVO_2$, $LiVO_3$ and VO_2 to temperatures ranging between 630 °C - 830 °C. A similar method was used to obtain $Li_{0.5}ZnV_{1.5}O_4$ [180].

Finally, the crystallographic and electronic properties of the solid solution $Li_{1-x}Zn_{2x}V_{2-x}O_4$ were recently described by Colemann et al. [139]. These spinels were obtained by heating mixtures of LiV_2O_4, ZnO and VO_2 to 750 °C under vacuum. The structure of the resulting material was described as $Li_{1-2x}Zn_{2x}[Li_xV_{2-x}]O_4$.

8.1.3 Spinel Preparation by Ion Exchange

This work proposes to introduce inc cations into LiV_2O_4 in order to stabilise the $[V_2]O_4$ framework of $Li_{1-x}V_2O_4$. A solid solution with the structure $(Li, Zn)_{8a}[V_2]_{16d}O_4$ is therefore considered most suitable.

Preliminary attempts to prepare solid solutions between LiV_2O_4 and ZnV_2O_4 at relatively high temperatures (600 °C) failed, largely because of the instability of the slightly lithium-deficient spinel $Li_{\sim 1.0}V_2O_4$ prepared according to the method described in Chapter 5.

At lower temperatures (300 °C - 400 °C), no reaction was observed between LiV_2O_4 and ZnV_2O_4. It therefore became necessary to consider other means of preparation, operative at temperatures within the stability range of $Li_{\sim 1.0}V_2O_4$.

Ion exchange reactions have been known for a long time in inorganic chemistry.

In 1963 Joubert and Durif [181] reported the formation of the spinel $Ge_3\square Zn_2O_8$ by ion exchange, according to the reaction:

$$Ge_3ZnLi_2O_8 + ZnSO_4 \rightarrow Ge_3\square Zn_2O_8 + Li_2SO_4$$

The ion exchange reaction is thus:

$$2Li^+ \longrightarrow Zn^{2+} + \square$$

In a subsequent paper, Joubert [158] described the preparation of a number of cation-deficient spinels by the ion exchange technique, e.g. $Co_2[M_3\square]O_8$, $ZnMn[M_3\square]O_8$ and $Zn_2[M_3\square]O_8$ (M = Ti, Ge). All these compounds are metastable and could not be prepared by the more conventional solid state reactions, i.e. directly from the metal oxides [158]. In this work, the preparation of zinc-doped LiV_2O_4 will be attempted, according to the ion exchange reaction:

$$LiV_2O_4 + xZnSO_4 \rightarrow Li_{1-2x}Zn_xV_2O_4 + xLi_2SO_4$$

The advantage of this method of preparation is the relatively low temperature range at which ion exchange may occur.

When compared to the high-temperature reactions described in the preceding section, this process suffers the disadvantage of creating vacancies within the spinel structure, which may have a destabilising effect.

This factor, however, should be of little importance in the context of this work, where vacancies are created in any case during the next step, i.e. delithiation of the spinel.

8.2 EXPERIMENTAL

The starting material, i.e. the lithium vanadium spinel, was prepared by the method outlined in Chapter 5. The cell constant was 8.237(2) Å, indicating a stoichiometry very close to $Li_{1.0}V_2O_4$. Zinc sulphate (Merck, analytical grade) was dried under vacuum at 300 °C for several hours. The zinc-doped spinel was prepared by ion exchange between stoichiometric quantities of LiV_2O_4 and $ZnSO_4$ in a sealed silica tube under vacuum. The mixture was allowed to react at 200 °C or 300 °C during a period of 9-11 days. The resulting powder was washed in water, to remove the Li_2SO_4 side-product, and dried in air. Lithium and zinc contents were obtained by atomic absorption analysis.

Lithium was extracted from $Li_xZn_yV_2O_4$ using a bromine solution as described in section 3.2.1. Stoichiometric quantities of Br_2 were used to obtain specific concentrations, excess amounts were employed to determine maximum delithiation. Reaction times varied between 1-5 days. Cyclic voltammetry experiments were carried out as described in section 3.3.2.

8.3 FORMATION OF $Li_xZn_yV_2O_4$ ($0.73<x<0.84$; $0.04<y<0.10$)

Compounds with the composition $Li_xZn_yV_2O_4$ ($0.73<x<0.84$, $0.04<y<0.10$) were prepared by ion exchange.

It was not possible to prepare samples with $y>0.10$, even when a large excess of $ZnSO_4$ was introduced. Table 8.1 gives the composition, temperature of preparation and cell constants of a few samples.

TABLE 8.1

Composition, temperature of preparation and cell constant of a few $Li_xZn_yV_2O_4$ samples

Composition	T_{prep} [°C]	a [Å]
$Li_{0.77}Zn_{0.04}V_2O_4$	300	8.245(2)
$Li_{0.73}Zn_{0.08}V_2O_4$	300	8.246(1)
$Li_{0.84}Zn_{0.05}V_2O_4$	200	8.245(2)
$Li_{0.78}Zn_{0.10}V_2O_4$	200	8.245(2)

Characteristic powder X-ray diffraction patterns of these phases are given in Figs 8.1 and 8.2. Traces of impurities, e.g. LiV_2O_5, could be detected in some samples. The $Li_xZn_yV_2O_4$ compounds display a cubic spinel pattern, with a relative intensity distribution typical of the $Li[M_2]O_4$ spinels. The patterns could be indexed to the cubic $Fd\bar{3}m$ space group; the cell constants showed a volume expansion of 0.3% with respect to the parent compound $Li_{\sim 1.0}V_2O_4$.

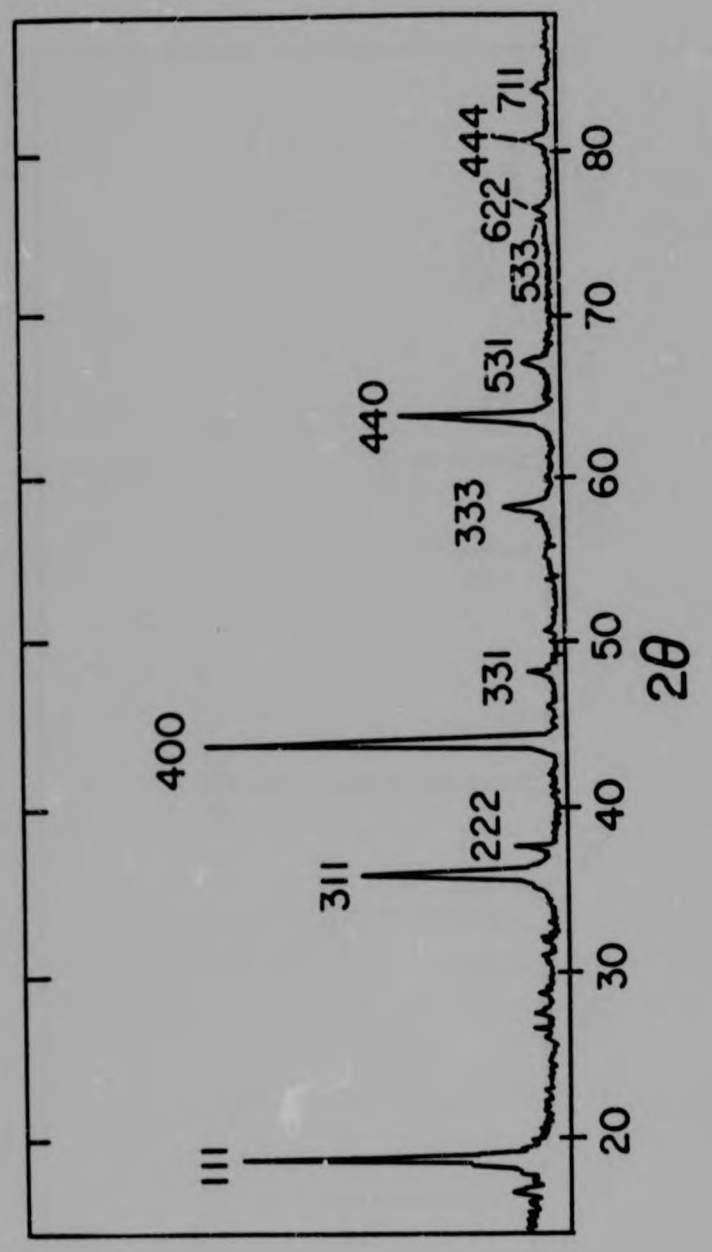

FIG. 8.1

X-ray diffraction pattern of $Li_{0.84}Zn_{0.05}V_2O_4$

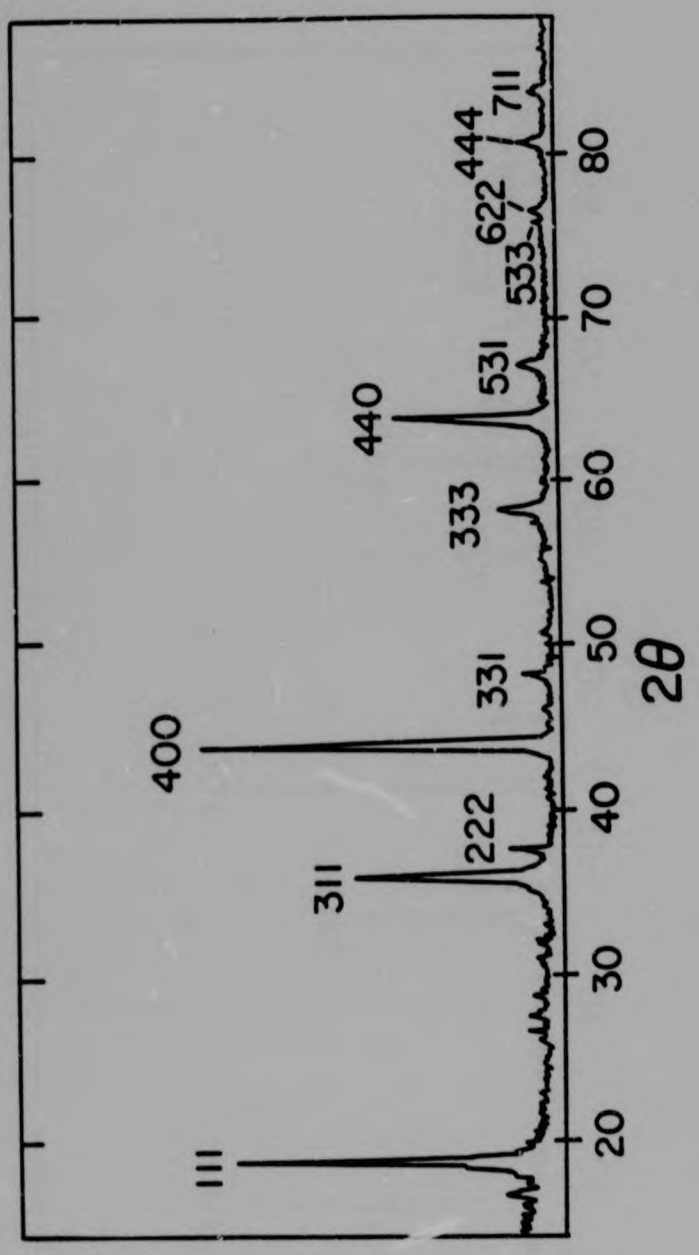

FIG. 8.1

X-ray diffraction pattern of $Li_{0.84}Zn_{0.05}V_2O_4$

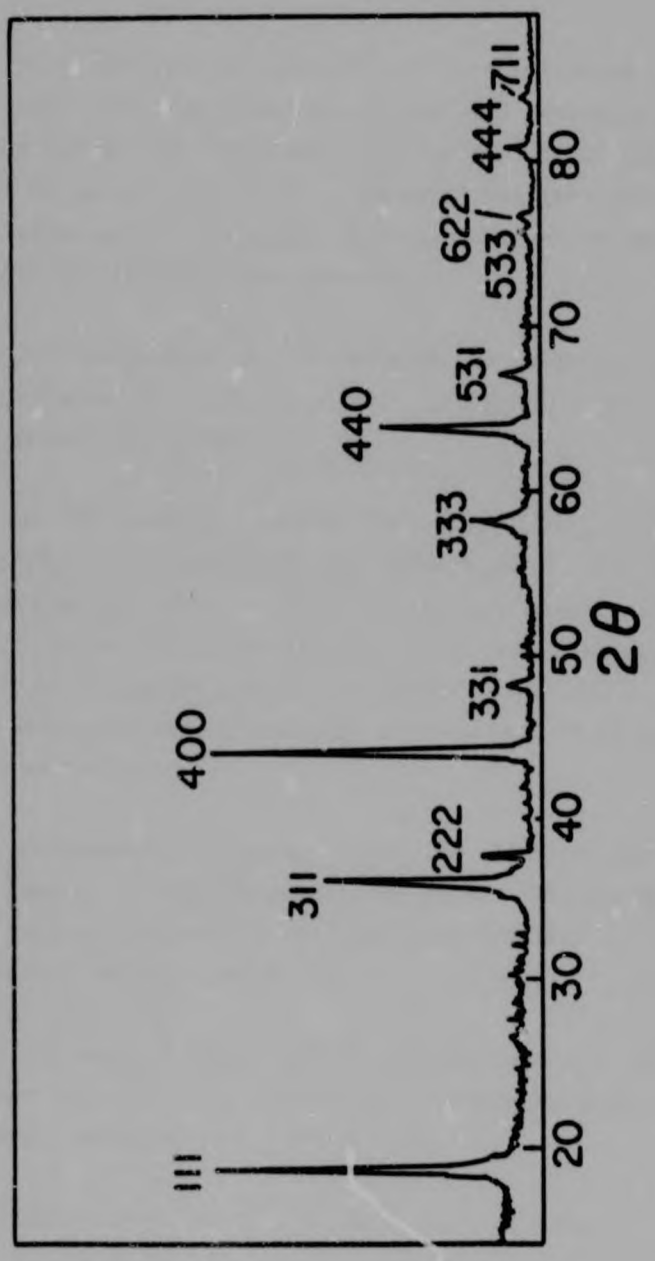

FIG. 8.2

X-ray diffraction pattern of $Li_{0.78}Zn_{0.10}V_2O_4$

8.4 STRUCTURE OF $Li_xZn_yV_2O_4$ (x ≈0.8, y ≈0.05)

The powder X-ray diffraction patterns of the zinc-doped lithium vanadium spinels were poorly defined. Peaks were generally broad, with numerous spikes and shoulders. The low quality of the X-ray patterns can be largely ascribed to compositional gradients within the particle, and to the small particle size of the material resulting from the ion exchange reaction.

Despite the poor appearance of the patterns, an intensity refinement was undertaken, in order to attempt to determine the structure of the zinc-doped spinel.

Two compounds of similar composition ($Li_{0.84}Zn_{0.05}V_2O_4$ and $Li_{0.77}Zn_{0.04}V_2O_4$) were selected for comparison. The powder X-ray diffraction patterns of these phases are given in Tables 8.2 and 8.3; since the X-ray patterns were very similar, only the pattern of $Li_{0.84}Zn_{0.05}V_2O_4$ is shown (Fig. 8.1). The refinements were carried out using 17 intensities, which corresponded to 24 reflections.

Preliminary refinements indicated that the lithium and zinc cations are located on the tetrahedral 8a sites. All attempts to place these cations in alternative positions resulted in an increase of the reliability factor.

In contrast, the exact location of the vanadium cations remained unclear. When divalent zinc cations are introduced into LiV_2O_4 by ion exchange, vacancies are formed:

$$xZnSO_4 + LiV_2O_4 \rightarrow Li^+_{1-2x}\square_x Zn^{2+}_x V_2O_4 + xLi_2SO_4$$

It was initially assumed (Model 1) that the vacancies would be found amongst the tetrahedral 8a sites, from which lithium was

TABLE 8.2

Powder X-ray diffraction pattern of $Li_{0.84}Zn_{0.05}V_2O_4$

Space group: $Fd3m(O_h^7)$ $a = 8.245(2)$ Å $\alpha = 90^0$

hkl	d^*_{obs} [Å]	d_{calc} [Å]	I^{**}_{obs}
111	4.764	4.760	897
311	2.484	2.486	747
222	2.381	2.380	95
400	2.061	2.061	1000
331	1.892	1.891	105
511	1.586	1.587	223
333	1.586	1.587	
440	1.459	1.457	576
531	1.393	1.394	131
533	-	1.257	93
622	-	1.243	78
444	1.189	1.190	118
551	-	1.154	85
711	-	1.154	
553	-	1.073	108
731	-	1.073	
800	-	1.031	76
751	-	0.952	133
555	-	0.952	
662	-	0.946	
840	-	0.922	150
753	-	0.905	71
911	-	0.905	
842	-	0.900	

* No d_{obs} is indicated for weak and diffuse peaks

** I_{obs} normalised to 1000

TABLE 8.3

Powder X-ray diffraction pattern of $Li_{0.77}Zn_{0.04}V_2O_4$

Space group: $Fd3m(O_h^7)$ $a = 8.245(2)$ Å $\alpha = 90^0$

hkl	d^*_{obs} [Å]	d_{calc} [Å]	I^{**}_{obs}
111	4.763	4.760	1000
311	2.485	2.486	806
222	2.380	2.380	99
400	2.062	2.061	917
331	-	1.892	98
511	1.588	1.587	195
333	1.588	1.587	
440	1.457	1.457	526
531	1.393	1.394	142
533	-	1.257	67
622	-	1.243	59
444	1.187	1.190	133
551	-	1.155	93
711	-	1.155	
553	-	1.073	101
731	-	1.073	
800	-	1.031	95
751	-	0.952	116
555	-	0.952	
662	-	0.946	
840	-	0.922	171
753	-	0.905	80
911	-	0.905	
842	-	0.900	

* No d_{obs} is indicated for weak and diffuse peaks

** I_{obs} normalised to 1000

removed by ion exchange. The predicted structure would thus be described by the expression:

$$(Li_{1-2x}Zn_x\square_x)_{8a}\,[V_2]_{16d}O_4$$

An intensity refinement was undertaken using this model. The cation occupancies and isotropic temperature factors were fixed at the values shown in Tables 8.4 and 8.5. The oxide anion B_{iso} factor and positional parameters were refined.

The structural parameters obtained for Model 1 are given in Tables 8.4 and 8.5. This model yielded the relatively high R values of 11.7% and 10.4% for the two compounds studied.

In the case of the lithium-deficient spinel $Li_{0.9}V_2O_4$, a fraction of the vanadium cations was found to occupy the tetrahedral 8a sites, whilst the vacancies were situated on the B sites (cf section 5.4). It was therefore postulated that a similar arrangement could be encountered in the zinc-substituted spinel, particularly if the starting material $Li_{\sim 1.0}V_2O_4$ is slightly lithium-deficient.

In model 2, the vanadium cations were allowed to occupy both the octahedral 16d sites and the tetrahedral 8a sites. The total vanadium content was restricted to 2.0. The anion B_{iso} factor and positional parameters were also refined. The isotropic temperature factors of all the cations and the 8a occupancies of the lithium and zinc ions were fixed as for Model 1.

The final structural parameters for Model 2 are listed in Tables 8.6 and 8.7. In the refined structure, 0.05(4) vanadium cations are situated in the 8a tetrahedra. Within experimental error, this would indicate that the tetrahedral A sites are entirely filled by a combination of Li^+, Zn^{2+} and V^{5+} cations.

TABLE 8.4

Structural parameters of $Li_{0.84}Zn_{0.05}V_2O_4$ (Model 1)

R = 11.7%

Space group: $Fd3m(O_h^7)$ a = 8.245(2) Å

Atom	Position	x	y	z	B[Å^2]	n
Li^+	8a	0.125	0.125	0.125	1.0	0.9
Zn^{2+}	8a	0.125	0.125	0.125	0.5	0.05
$V^{3+/4+}$	16d	0.500	0.500	0.500	1.0	2.0
O^{2-}	32e	0.254(2)	0.254(2)	0.254(2)	2.4(8)	4.0

TABLE 8.5

Structural parameters of $Li_{0.77}Zn_{0.04}V_2O_4$ (Model 1)

R = 10.4%

Space group: $Fd3m(O_h^7)$ a = 8.245(2) Å

Atom	Position	x	y	z	B[Å^2]	n
Li^+	8a	0.125	0.125	0.125	1.0	0.8
Zn^{2+}	8a	0.125	0.125	0.125	0.5	0.05
$V^{3+/4+}$	16d	0.500	0.500	0.500	0.5	2.0
O^{2-}	32e	0.254(2)	0.254(2)	0.254(2)	2.1(7)	4.0

The reliability factors obtained for this model were 11.9% and 8.9% in the case of $Li_{0.84}Zn_{0.05}V_2O_4$ and $Li_{0.77}Zn_{0.04}V_2O_4$ respectively. Model 2 thus represents an improvement over Model 1 only in the case of $Li_{0.77}Zn_{0.04}V_2O_4$.

The third possibility envisaged comprises a distribution of the vanadium cations in the two sets of octahedral sites, namely the 16c and the 16d sites (Model 3). The refinement was carried out as for model 2, with vanadium cations in the 16c and 16d octahedra.

TABLE 8.6

Structural parameters of $Li_{0.84}Zn_{0.05}V_2O_4$ (Model 2)

R = 11.9%

Space group: $Fd3m(O_h^7)$ a = 8.245(2) Å

Atom	Position	x	y	z	B[Å^2]	n
Li^+	8a	0.125	0.125	0.125	1.0	0.9
Zn^{2+}	8a	0.125	0.125	0.125	0.5	0.05
$V^{3+/4+}$	16d	0.500	0.500	0.500	0.5	1.95(4)
V^{5+}	8a	0.125	0.125	0.125	0.5	0.05(4)
O^{2-}	32e	0.255(2)	0.255(2)	0.255(2)	2.5(6)	4.0

TABLE 8.7

Structural parameters of $Li_{0.77}Zn_{0.04}V_2O_4$ (Model 2)

R = 8.9%

Space group: $Fd3m(O_h^7)$ a = 8.245(2) Å

Atom	Position	x	y	z	B[Å^2]	n
Li^+	8a	0.125	0.125	0.125	1.0	0.8
Zn^{2+}	8a	0.125	0.125	0.125	0.5	0.05
$V^{3+/4+}$	16d	0.500	0.500	0.500	0.5	1.96(4)
V^{5+}	8a	0.125	0.125	0.125	0.5	0.04(4)
O^{2-}	32e	0.254(2)	0.254(2)	0.254(2)	2.2(8)	4.0

The full structural parameters obtained for this model are given in Tables 8.8 and 8.9. In $Li_{0.84}Zn_{0.05}V_2O_4$, a structure where 0.13(3) $V^{3+/4+}$ cations occupy the 16c sites gave the greatly improved R = 7.6%. However, in $Li_{0.77}Zn_{0.04}V_2O_4$ only 0.07(4) vanadium ions were placed in the 16c sites, yielding an indifferent R value of 11.1%.

TABLE 8.8

Structural parameters of $Li_{0.84}Zn_{0.05}V_2O_4$ (Model 3)

R = 7.6%

Space group: $Fd3m(O_h^7)$ a = 8.245(2) Å

Atom	Position	x	y	z	B[Å^2]	n
Li^+	8a	0.125	0.125	0.125	1.0	0.9
Zn^{2+}	8a	0.125	0.125	0.125	0.5	0.05
$V^{3+/4+}$	16d	0.500	0.500	0.500	0.5	1.87(3)
$V^{3+/4+}$	16c	0.000	0.000	0.000	0.5	1.13(3)
O^{2-}	32e	0.255(1)	0.255(1)	0.255(1)	3.6(6)	4.0

TABLE 8.9

Structural parameters of $Li_{0.77}Zn_{0.04}V_2O_4$ (Model 3)

R = 11.1%

Space group: $Fd3m(O_h^7)$ a = 8.245(2) Å

Atom	Position	x	y	z	B[Å^2]	n
Li^+	8a	0.125	0.125	0.125	1.0	0.8
Zn^{2+}	8a	0.125	0.125	0.125	0.5	0.05
$V^{3+/4+}$	16d	0.500	0.500	0.500	0.5	1.93(4)
$V^{3+/4+}$	16c	0.000	0.000	0.000	0.5	0.07(4)
O^{2-}	32e	0.256(2)	0.256(2)	0.256(2)	2.8(8)	4.0

Owing to the severe lack of agreement between the two sets of data, a definite conclusion on the exact structure of $Li_{\sim 0.8}Zn_{\sim 0.05}V_2O_4$ cannot be drawn.

However, a few trends are verified in both cases, and can therefore be accepted with a fair degree of confidence. Firstly, both the lithium and the zinc cations occupy the tetrahedral sites. This is not surprising, given the strong tendency towards tetrahedral coordination of the zinc cations; moreover, a major rearrangement of the lithium cations is not expected to occur, since only a very limited amount of Zn^{2+} is introduced.

Secondly, the bulk of the vanadium cations are located on the B sites of the spinel. A 'normal' spinel structure is thus confirmed for $Li_{\sim 0.8}Zn_{\sim 0.05}V_2O_4$.

The exact position of the vacancies in the zinc-doped spinel could not be determined. Although vacancies are generally found amongst the octahedral sites in oxo-spinels, as in $Li_{0.9}V_2O_4$ (cf Chapter 5), this trend could be neither confirmed nor disproved in $Li_{\sim 0.8}Zn_{\sim 0.05}V_2O_4$, due to the poor quality of the data.

8.5 LITHIUM EXTRACTION FROM $Li_xZn_yV_2O_4$ ($0.73<x<0.84$; $0.04<y<0.10$)

8.5.1 Results

As in the case of LiV_2O_4, lithium can be extracted from the zinc-doped compound $Li_{1-y}Zn_yV_2O_4$ ($0.05<y<0.10$) by chemical oxidation, using a bromine solution. The lowest lithium content reached in these experiments, $Li_{0.20}Zn_{0.02}V_2O_4$, was comparable to that obtained with the undoped material. Table 8.10 lists a few typical results.

As is evident from the data presented in Table 8.10, within experimental error, lithium ions alone are extracted up to a composition of $Li_{0.64}Zn_{0.04}V_2O_4$. For lower lithium concentrations, zinc extraction occurs concurrently: in samples where maximum chemical delithiation is attained, practically all the Zn^{2+} ions are also removed.

Although electrostatic forces between cations and anions should be twice as strong in the case of Zn^{2+} when compared to Li^+, the small size of the zinc cation probably facilitates its extraction. The presence of numerous vacancies in the partially delithiated compound is also expected to increase the mobility of the zinc cations.

TABLE 8.10

Results of lithium extraction from $Li_xZn_yV_2O_4$

Starting material	Composition of end-product ($Li_xZn_yV_2O_4$)		Reaction time	Lattice constant a [Å]
	x	y		
$Li_{0.84}Zn_{0.05}V_2O_4$	0.65	0.04	24 hrs	8.223(3)
"	0.64	0.04	"	8.230(2)
"	0.60	0.03	"	8.224(3)
"	0.53	0.02	"	8.224(3)
"	0.34	0.01	5 days	-
$Li_{0.78}Zn_{0.10}V_2O_4$	0.31	0.03	"	-
$Li_{0.73}Zn_{0.08}V_2O_4$	0.20	0.02	"	-
$Li_{0.77}Zn_{0.04}V_2O_4$	0.21	0.01	"	-

8.5.2 Structure

Characteristic powder X-ray diffraction patterns of a few delithiated compounds are shown in Figs 8.3 - 8.5. A gradual loss of crystallinity is noticeable as delithiation progresses. This is due partly to an increase of the amorphous nature of the material, and partly to the break-up of the particles.

It is immediately apparent that the spinel pattern is maintained, at least up to a stoichiometry $Li_{0.53}Zn_{0.02}V_2O_4$: lattice constants of samples up to this composition indicate that the unit cell remains cubic, with a volume contraction of less than one percent. Cell constants of samples with a lower lithium content could not be determined owing to their poor crystallinity.

In view of the lack of success in the structure determination of the parent compound, no structure refinements were attempted. However, a few conclusions can be drawn. The general appearance

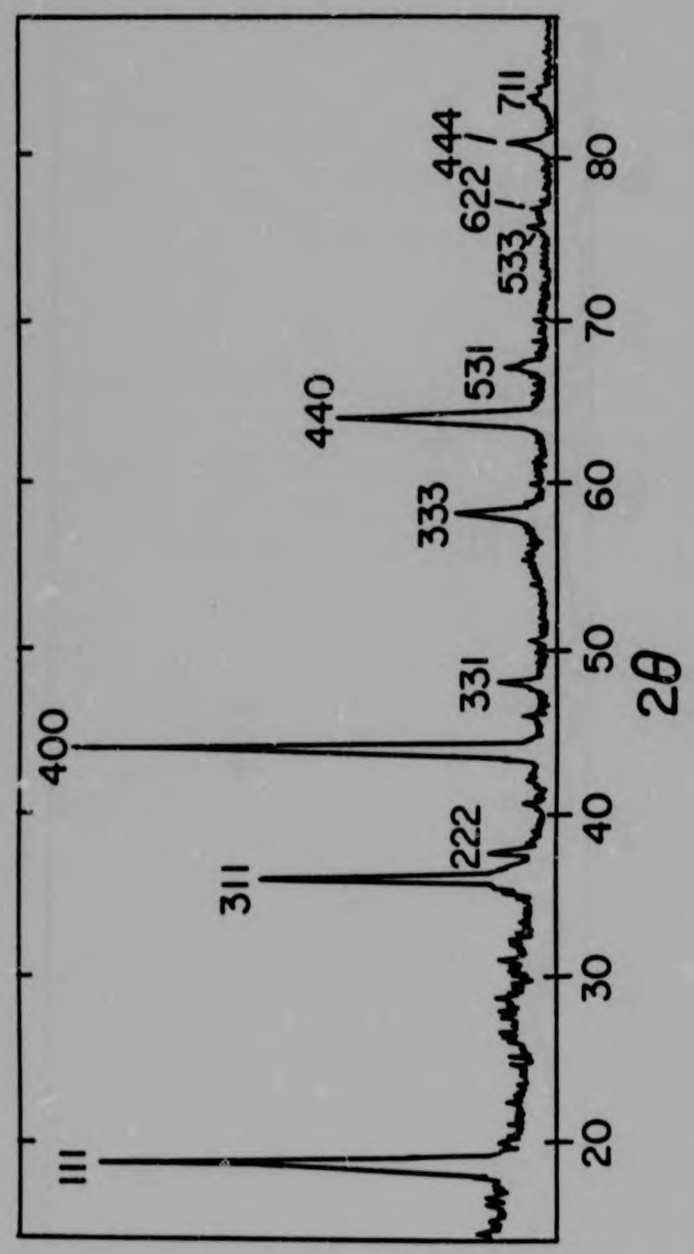

FIG. 8.3
X-ray diffraction pattern of $Li_{0.65}Zn_{0.04}V_2O_4$

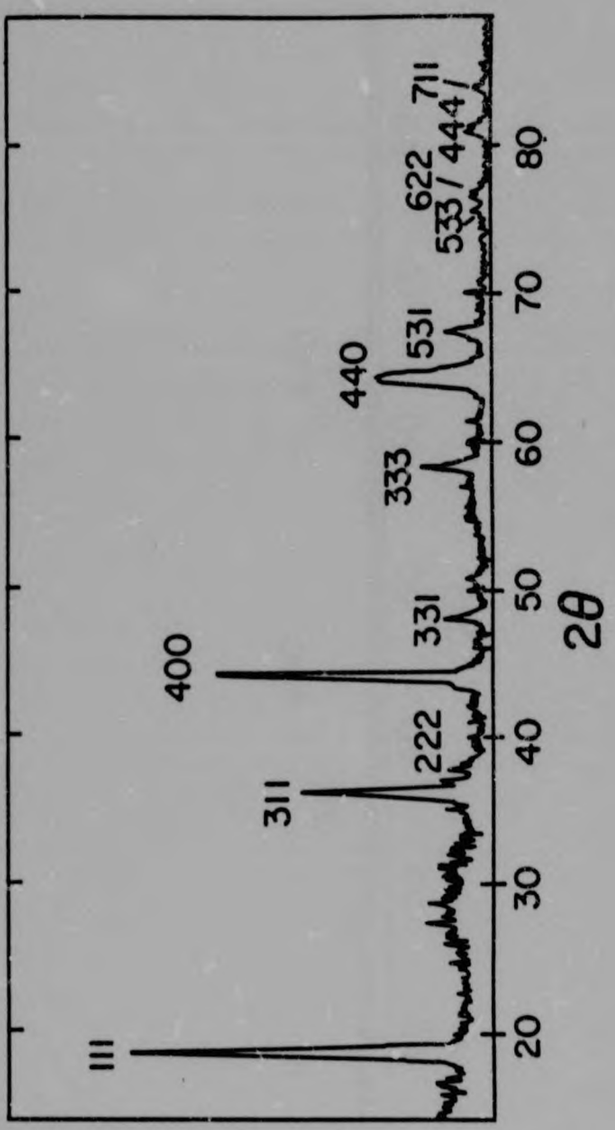

FIG. 8.4

X-ray diffraction pattern of $Li_{0.53}Zn_{0.02}V_2O_4$

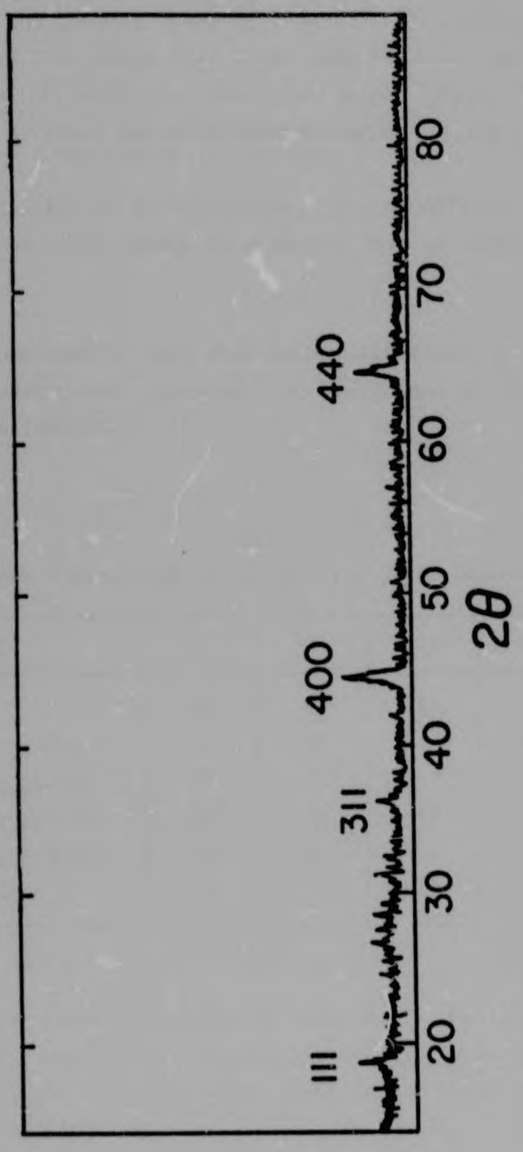

FIG. 8.5
X-ray diffraction pattern of $Li_{0.34}Zn_{0.01}V_2O_4$

of the patterns corresponds to an oxide spinel pattern. More importantly, the overall symmetry remains cubic, without any clear splitting of the peaks. Both these observations indicate, with a fair degree of certainty, that the spinel $[V_2]O_4$ framework is maintained at least up to the stoichiometry $Li_{0.53}Zn_{0.02}V_2O_4$.

Further delithiation is accompanied by a significant decrease of zinc cations: this leads to a severe loss of crystallinity (cf Fig. 8.5).

A few intensities of the strongest reflections of various delithiated zinc-doped compounds, of LiV_2O_4 and of $Li_{0.28}V_2O_4$ are compared in Table 8.11.

TABLE 8.11

Peak intensities for a few $Li_xZn_yV_2O_4$ compounds

Compound	111	311	222	400	440
LiV_2O_4	108	45	15	100	38
$Li_{0.84}Zn_{0.05}V_2O_4$	85	55	13	100	45
$Li_{0.65}Zn_{0.05}V_2O_4$	89	57	9	100	44
$Li_{0.53}Zn_{0.02}V_2O_4$	97	58	12	100	42
$Li_{0.34}Zn_{0.01}V_2O_4$	55	40	<10	100	65
$Li_{0.28}V_2O_4$	35	25	4	100	72

As it can be immediately seen in Table 8.11, the relative intensities of delithiated compounds up to the stoichiometry $Li_{0.53}Zn_{0.02}V_2O_4$ are remarkably similar to those of a characteristic starting material, $Li_{0.84}Zn_{0.05}V_2O_4$. This further confirms that the spinel $[V_2]O_4$ framework is indeed retained, at least up to $Li_{0.53}Zn_{0.02}V_2O_4$.

In contrast, the relative intensities of $Li_{0.34}Zn_{0.01}V_2O_4$ are intermediate between the values for the zinc-doped spinel compounds and undoped $Li_{0.28}V_2O_4$. This would indicate that some migration of vanadium cations through the layers occurs for low lithium concentrations, and probably leeds to a vanadium ion distribution intermediate between the cubic $[V_2]O_4$ framework and undoped $Li_{0.28}V_2O_4$.

8.6 CYCLIC VOLTAMMETRY OF $Li_{0.77}Zn_{0.08}V_2O_4$

Cyclic voltammetry experiments were carried out in order to characterise the insertion and extraction reactions of lithium with the zinc-doped spinel from an electrochemical point of view. In particular, this technique allows a rapid assessment of the reversibility of the delithiation reaction.

For the sake of completeness, lithium insertion into $Li_{0.77}Zn_{0.08}V_2O_4$ was also examined by cyclic voltammetry. A voltammogram obtained at a scan rate v = 1 mV/sec is shown in Fig. 8.6. The lithiation process is characterised by a single broad peak, with I_{max} at a potential of 2.18 V. The reaction is reversible, with an oxidation peak at E = 2.62 V. The second cycle is practically identical to the first one. This voltammogram is very similar to that obtained in the case of the unsubstituted material $Li_{1+x}V_2O_4$ (cf section 7.5.2), except for the flattened shape of the oxidation peak in the case of Zn^{2+}-containing compound, which could be due to a slower diffusion rate in $Li_{2-2y}Zn_yV_2O_4$.

A cyclic voltammogram with an initial anodic scan (v = 1 mV/sec) is shown in Fig. 8.7. A broad peak at 3.66 V corresponds to the delithiation reaction. Both the shape and the position of this oxidation peak are very similar to those observed in the case of $Li_{1-x}V_2O_4$ (Fig. 7.8). Upon scan reversal, only a weak and diffuse peak is observed at ca. 1.62 V, indicating that the reaction

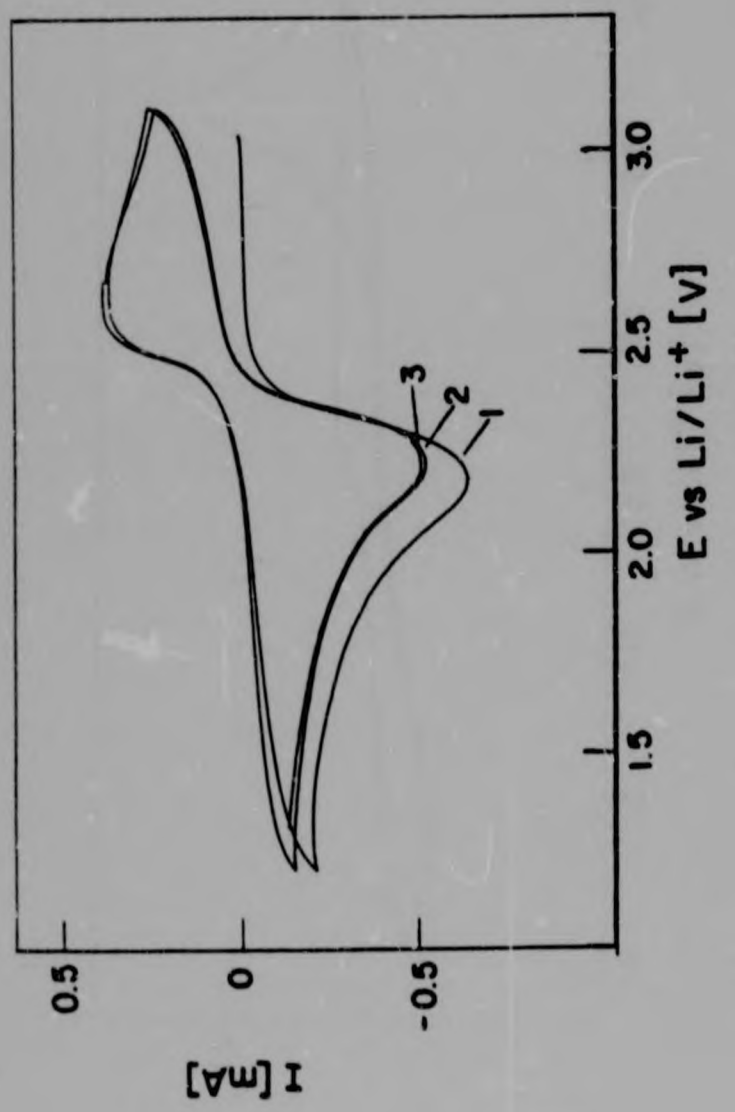

FIG. 8.6

Cyclic voltammogram of the system $Li_{0.77+x}Zn_{0.08}V_2O_4$

(initial scan cathodic; v = 1 mV/sec)

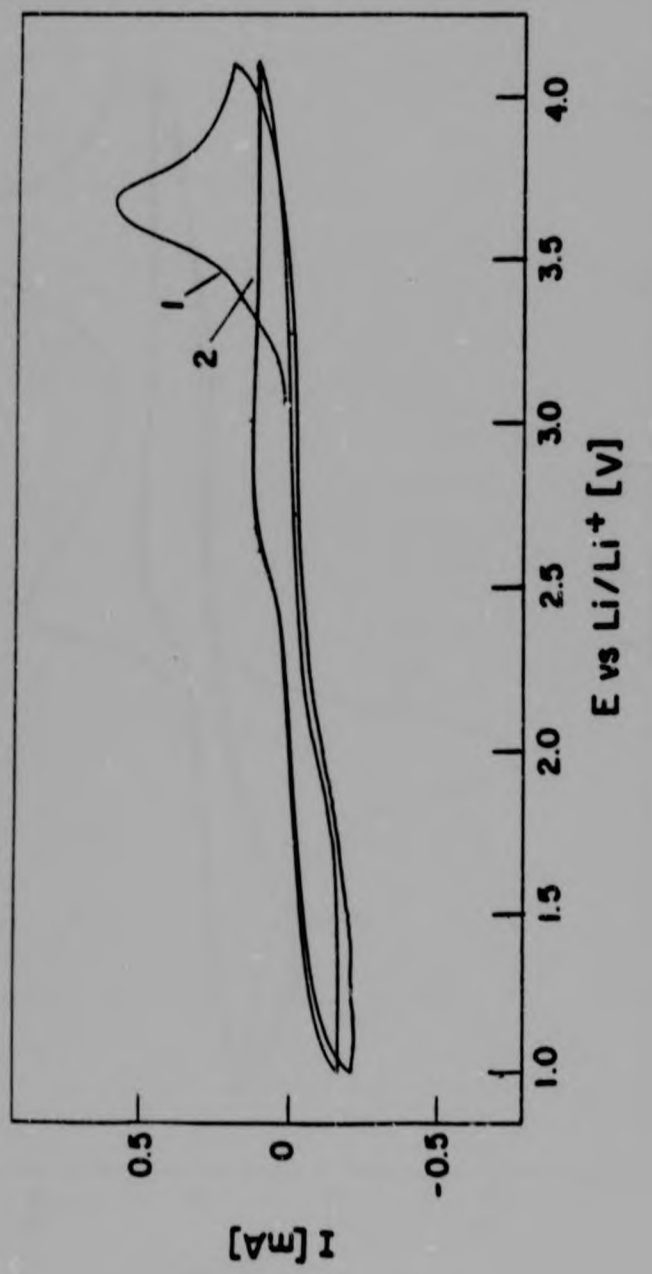

FIG. 8.7
Cyclic voltammogram of the system $Li_{0.77\pm x}Zn_{0.08}V_2O_4$
(initial scan anodic; v = 1 mV/sec)

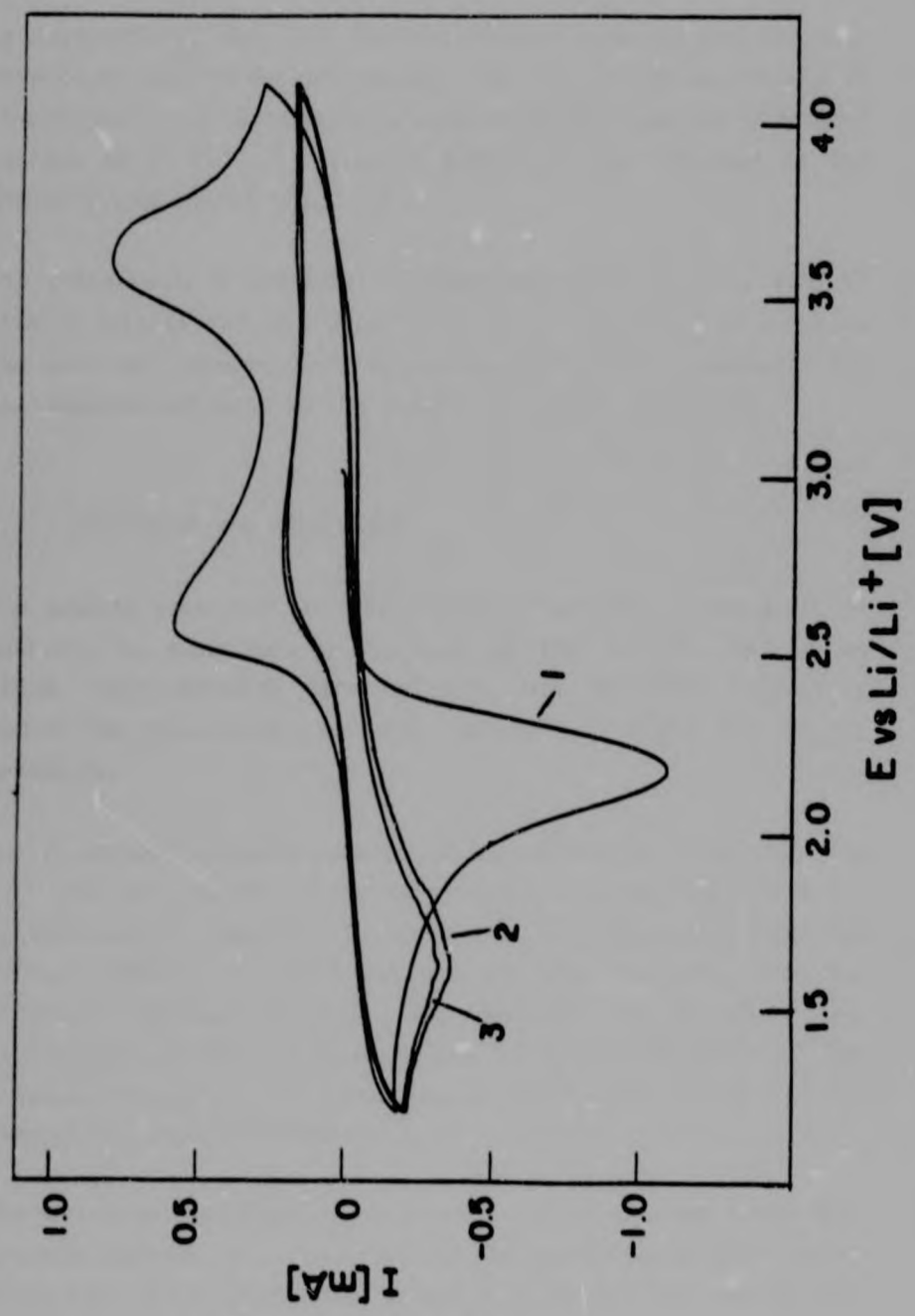

FIG. 8.8
Cyclic voltammogram of the system $Li_{0.77\pm x}Zn_{0.08}O_4$
(initial scan cathodic; v = 1 mV/sec)

is irreversible, but that the delithiated compound can be relithiated by a different mechanism. The new lithiation process is reversible; the corresponding weak oxidation peak has a current maximum at 2.79 V. A similar behaviour was observed in the unsubstituted spinel (Fig. 7.8).

For comparison, a complete voltammogram (1.20 V < E < 4.10 V) with an initial cathodic scan is shown in Fig. 8.8. It exhibits the combined features described above, and strongly resembles the voltammogram obtained in the case of $Li_{1\pm x}V_2O_4$ (Fig. 7.9).

8.7 DISCUSSION AND CONCLUSION

The results presented in this chapter show that, although it is possible to substitute a fraction of the lithium cations in LiV_2O_4 with divalent zinc cations, the resulting $Li_xZn_yV_2O_4$ cannot be delithiated entirely without affecting the $[B_2]X_4$ framework.

The structural characterisation of the materials shows that the Zn^{2+} ions are located in the 8a tetrahedral sites (section 8.4), as anticipated. However, in the course of delithiation, for low lithium content, the Zn^{2+} cations are also extracted from the structure (section 8.5.1). The decrease of the zinc- and lithium-ion content is accompanied by a rearrangement of the vanadium ions within the structure, as previously observed in the case of $Li_{1-x}V_2O_4$ (chapter 7).

The structural modification is reflected by the powder X-ray diffraction pattern (Fig. 8.5) and by the cyclic voltammetry study (Figs 8.7 - 8.8). The latter shows conclusively that the delithiation of $Li_{0.77}Zn_{0.08}V_2O_4$ is irreversible, due to the loss of the $[B_2]X_4$ framework.

The partial substitution of Li^+ with Zn^{2+} does not affect significantly the electrochemical characteristics of the insertion/extraction reactions. The peak potentials, intensities and shapes are essentially the same as those observed in the case of the unsubstituted spinel LiV_2O_4.

It can therefore be concluded that partial substitution of Li^+ with Zn^{2+} cations in LiV_2O_4 only achieves stabilisation of the $[B_2]X_4$ framework in delithiated compounds with a relatively high lithium content. The oxidation potential required to extract lithium from the spinel is sufficiently high to displace concurrently the less mobile, divalent zinc cations, situated within the 8a-16c-8a channels of the $[B_2]X_4$ sub-lattice.

CHAPTER 9

ELECTROSTATIC ENERGY OF THE LITHIATED SPINELS $Li_xMn_3O_4$ and $Li_{1+x}Mn_2O_4$ $(0<x\leq1)$

9.1 INTRODUCTION

Hitherto, studies of the insertion of lithium into spinel compounds [26,28,33,78] have focused primarily on the compositional range and structure of the products and on the lithiation mechanism.

Clearly, the electrochemical potential, ion mobility and lattice energy must play an important part in determining the lithiation mechanism and the reactivity towards insertion of spinels of different composition.

An investigation of the variation of lattice energy with lithiation is expected to enable us to predict the most stable structure of the lithiated spinel $LiAB_2X_4$, and would thereby further our understanding of the mechanism of lithium insertion into spinels.

The calculation of the total lattice energy of a complex structure is usually difficult, owing to the unavailability of precise data relating to the physical properties of the individual compounds. For this reason, the electrostatic (or coulombic) energy is frequently used as an acceptable approximation of the lattice energy.

The calculations were carried out on well-characterised lithium-rich spinels $Li_xMn_3O_4$ and $Li_{1+x}Mn_2O_4$, where $0<x\leq1$ [33]. Hausmannite (Mn_3O_4) was chosen as being representative of AB_2O_4 spinels, where A and B are first row transition metals; prelimi-

nary results for $Li_xFe_3O_4$ ($0<x\leq1$) strongly resembled those described in this chapter for $Li_xMn_3O_4$. The compound $LiMn_2O_4$ was selected as an example of the isostructural spinels $Li[M_2]O_4$ (M = Mn, Ti, V) which have been shown to incorporate lithium [33,78].

9.2 LATTICE ENERGY IN IONIC CRYSTALS

The lattice energy of an ionic crystal is the energy which is released when a mole of ions are brought together from an infinite distance to form a regular array in a crystal; it consists mainly of the electrostatic or coulombic energy and of the repulsion energy, which together account for over 90% of the total energy of the crystal.

The electrostatic interaction between a pair of ions with charges q_1 and q_2, separated by a distance r, is expressed by the coulombic force:

$$F = \frac{q_1 \cdot q_2}{r^2} \qquad (9.1)$$

or by the potential:

$$U = -\frac{q_1 \cdot q_2}{r} \qquad (9.2)$$

As the two charges are brought close together, the mutual repulsion between the two positively charged nuclei and the two negatively charged electron clouds becomes manifest. According to the Born-Mayer model [182], this energy may be expressed by the potential:

$$U = b \cdot e^{-r/a} \qquad a,b = \text{constants} \qquad (9.3)$$